LUND UNIVERSITY

Experimental and Numerical Investigations of Heat Transfer related to Gas Turbine Applications

Hussain, Safeer

2019

Document Version:
Publisher's PDF, also known as Version of record

Link to publication

Citation for published version (APA):
Hussain, S. (2019). *Experimental and Numerical Investigations of Heat Transfer related to Gas Turbine Applications*. Department of Energy Sciences, Lund University.

Total number of authors:
1

General rights
Unless other specific re-use rights are stated the following general rights apply:
Copyright and moral rights for the publications made accessible in the public portal are retained by the authors and/or other copyright owners and it is a condition of accessing publications that users recognise and abide by the legal requirements associated with these rights.
• Users may download and print one copy of any publication from the public portal for the purpose of private study or research.
• You may not further distribute the material or use it for any profit-making activity or commercial gain
• You may freely distribute the URL identifying the publication in the public portal

Read more about Creative commons licenses: https://creativecommons.org/licenses/

Take down policy
If you believe that this document breaches copyright please contact us providing details, and we will remove access to the work immediately and investigate your claim.

LUND UNIVERSITY

PO Box 117
221 00 Lund
+46 46-222 00 00

Experimental and Numerical Investigations of Heat Transfer related to Gas Turbine Applications

SAFEER HUSSAIN
FACULTY OF ENGINEERING | LUND UNIVERSITY

Experimental and Numerical Investigations of Heat Transfer related to Gas Turbine Applications

Safeer Hussain

LUNDS UNIVERSITET
Lunds Tekniska Högskola

DOCTORAL DISSERTATION

by due permission of the Faculty of Engineering (LTH), Lund University, Sweden. To be publicly defended on Tuesday 11 June 2019, at 10:15 AM in Lecture Hall M: B in the M-building, Ole Römers väg 1, Lund, Sweden.

Faculty opponent

Associate Professor David Gillespie

Department of Engineering Science,

University of Oxford, Oxford, U.K.

Organization LUND UNIVERSITY	Document name DOCTORAL DISSERTATION
Department of Energy Sciences	Date of issue June 11, 2019
Author(s) Safeer Hussain	Sponsoring organization Higher Education Commission (HEC) of Pakistan

Title and subtitle

Experimental and Numerical Investigations of Heat Transfer related to Gas Turbine Applications

Abstract

Gas turbines are broadly used in aerospace and marine propulsion and power production etc. Investigation of heat transfer in gas turbines is a long-lasting and still an active subject of research due to its tremendous importance. Thermal efficiency, durability and fatigue lifetime of a gas turbine greatly rely on the heat transfer characteristics of gas turbine components. According to the first law of thermodynamics, efficiency of a gas turbine can be increased by increasing the gas turbine inlet temperature (TIT) and minimizing the losses occurring in the gas turbine. To permit high TIT in gas turbines, a sophisticated gas turbine system with high cooling ability and minimum losses is required.

With the objective of high thermal efficiency, initially as a fundamental study, a pair of vortex generator (VG) was imbedded in a boundary layer upstream of a cylindrical obstacle. There are well established vortical structures associated with an obstacle positioned in the flow and similarly with a vortex generator (VG). This has been designed with an idea how the vortices accompanied by the obstacle and VG interact with each other and consequently how the heat transfer characteristics on the endwall is affected. The orientation, position and yaw angle of attack were studied experimentally using the steady state liquid thermography method. The study of orientation of VG revealed that counter flow inward (CFI) orientation is useful for endwall heat transfer augmentation whereas, counter flow outward (CFO) orientation is appropriate for reduction of heat transfer on the endwall. Moreover, the position of the VG relative to the obstacle also influenced the endwall heat transfer and more importantly, a 45° angle of attack provided larger augmentation of heat transfer than a lower angle of attack.

Employing the results of this study, a VG pair installed in CFO orientation upstream of an airfoil was investigated with the objective to suppress the heat transfer and horseshoe vortex (HV) in the junction region of a nozzle guide vane. The high heat transfer in the junction region results a hot spot and moreover, the HV increases the secondary losses in the gas turbine. The VG pair was separated apart at different gaps in the spanwise direction making different cases. The experimental results showed reduction of endwall heat transfer in the junction region with the VG pair. Moreover, numerical simulations using ANSYS Fluent predicted similar behavior of heat transfer and the flow features showed suppression of the secondary flow particularly the HV with the presence of the VG compared to without VG case.

Similarly, utilizing the knowledge gained in the fundamental study, VGs were used for thermal performance enhancement of pin fins which are usually employed in the heat transfer augmentation for internal cooling of the trailing part of a gas turbine blade/vane. Vortex generators were mounted in pairs upstream of the first row of in-line pin fins arrays. Thermal performance obtained numerically was compared without VGs and with VGs positioned at various locations with reference to the pin fins and yaw angles for various Reynolds numbers. The results illustrated that thermal performance was enhanced with VGs irrespective of the VG angle and position compared to the case without VGs. However, the level of enhancement is dependent on the VGs angle and position. The VG placed at 45° with a moderate gap between VGs and pin fins showed greater thermal performance.

In advanced gas turbines, the assembly of different components of the gas turbine may lead to some modifications in the flow paths. In an aero engine, when a low pressure turbine is connected to the nozzle section which has outlet guide vanes, a cavity is generated as a result of the assembly process. This cavity is formed upstream of an outlet guide vane. Different streamwise distances between the cavity and outlet guide vane (in this study an airfoil is considered) were investigated experimentally as well as numerically. Results demonstrated that the cavity located at a small distance is favorable as it considerably reduced the endwall heat transfer in the junction region of the airfoil. Similarly, the meeting parts of combustor and turbine are assembled via an axisymmetric contouring to match the diameters of both parts. So the effect of an axisymmetric endwall contouring on film cooling/heat transfer and secondary losses was numerically investigated for a nozzle guide vane (NGV) in a single passage region. It was revealed that an axisymmetric contouring enhanced the film cooling effectiveness. The heat transfer increased with the addition of film cooling which is obvious but the level of enhancement degraded with endwall contouring. Flow structures highlighted the suppression of the secondary flow.

Key words:

heat transfer, obstacle, vortex generator, pin fins, endwall, Nusselt number, thermal performance, film cooling effectiveness, contouring.

Classification system and/or index terms (if any)

Supplementary bibliographical information		Language English
ISSN and key title ISSN 0282-1990 ISRN LUTMDN/TMHP-19/1145-SE		ISBN 978-91-7895-048-5 (print) 978-91-7895-049-2 (pdf)
Recipient's notes	Number of pages 74	Price
	Security classification	

I, the undersigned, being the copyright owner of the abstract of the above-mentioned dissertation, hereby grant to all reference sources permission to publish and disseminate the abstract of the above-mentioned dissertation.

Signature  Date May 02, 2019

Experimental and Numerical Investigations of Heat Transfer related to Gas Turbine Applications

Safeer Hussain

Department of Energy Sciences

Faculty of Engineering (LTH)

Lund University, Lund, Sweden

www.energy.lth.se

Thesis for the degree of Doctor of Philosophy in Engineering.

©Safeer Hussain, 2019

Division of Heat Transfer
Department of Energy Sciences
Faculty of Engineering (LTH)
Lund University
Box 118
SE-221 00 LUND
SWEDEN

978-91-7895-048-5 (print)
978-91-7895-049-2 (pdf)
ISRN: LUTMDN/TMHP-19/1145-SE
ISSN: 0282-1990

Printed in Sweden by Media-Tryck, Lund University
Lund 2019

Popular Science

Gas turbines are used in many engineering applications like aero engine and land based power production etc. Efficiency of the gas turbines greatly depends on the operational temperature. Therefore, typically gas turbines operate at high temperature and moreover advanced gas turbines operate far above the allowable limit of the material which is made possible by cooling the gas turbine. Therefore, cooling of gas turbines is vital for safe operation of the device. The cooling air is extracted from the compressor. There is a continuous struggle to increase the gas turbine temperature more in order to achieve higher thermal efficiency. This could be possible by design of a sophisticated cooling system that has characteristics of high heat transfer and less amount of coolant. In addition, cooling is divided into two types called internal and external cooling.

For internal cooling, different mechanisms are used to disturb the cooling air and as a result heat transfer is enhanced. In the trailing part of the gas turbine blade/vane usually pin fins are employed for heat transfer augmentation. Similarly, for external cooling, film cooling is used to provide a protective layer between the hot gases and metallic wall.

A junction is formed when a gas turbine blade/vane is attached to the hub wall, and the flow approaching to the junction region turns into various vortical flow patterns. This vortical flow is called secondary flow. Due to the vortical flow in the upstream junction region, the hot gases impinge on the wall and increases the heat transfer to a very high level and also it causes severe pressure drop. Therefore, typically film cooling is employed in the junction region of gas turbine blade/vane. By controlling the secondary flow in the junction region, heat transfer and pressure losses can be controlled.

In this thesis, with an objective to promote the gas turbine efficiency, studies were conducted with different perspectives of gas turbines by starting from a fundamental study to more real studies in gas turbines. The study comprised experimental as well as numerical investigations. The results presented in this study are promising for the improvement of gas turbine cooling performance and reduction of secondary losses which both are equally important for the enhancement of gas turbine performance.

Abstract

Gas turbines are broadly used in aerospace and marine propulsion and power production etc. Investigation of heat transfer in gas turbines is a long-lasting and still an active subject of research due to its tremendous importance. Thermal efficiency, durability and fatigue lifetime of a gas turbine greatly rely on the heat transfer characteristics of gas turbine components. According to the first law of thermodynamics, efficiency of a gas turbine can be increased by increasing the gas turbine inlet temperature (TIT) and minimizing the losses occurring in the gas turbine. To permit high TIT in gas turbines, a sophisticated gas turbine system with high cooling ability and minimum losses is required.

With the objective of high thermal efficiency, initially as a fundamental study, a pair of vortex generator (VG) was imbedded in a boundary layer upstream of a cylindrical obstacle. There are well established vortical structures associated with an obstacle positioned in the flow and similarly with a vortex generator (VG). This has been designed with an idea how the vortices accompanied by the obstacle and VG interact with each other and consequently how the heat transfer characteristics on the endwall is affected. The orientation, position and yaw angle of attack were studied experimentally using the steady state liquid thermography method. The study of orientation of VG revealed that counter flow inward (CFI) orientation is useful for endwall heat transfer augmentation whereas, counter flow outward (CFO) orientation is appropriate for reduction of heat transfer on the endwall. Moreover, the position of the VG relative to the obstacle also influenced the endwall heat transfer and more importantly, a 45^{o} angle of attack provided larger augmentation of heat transfer than a lower angle of attack.

Employing the results of this study, a VG pair installed in CFO orientation upstream of an airfoil was investigated with the objective to suppress the heat transfer and horseshoe vortex (HV) in the junction region of a nozzle guide vane. The high heat transfer in the junction region results a hot spot and moreover, the HV increases the secondary losses in the gas turbine. The VG pair was separated apart at different gaps in the spanwise direction making different cases. The experimental results showed reduction of endwall heat transfer in the junction region with the VG pair. Moreover, numerical simulations using ANSYS Fluent predicted similar behavior of heat transfer and the flow features showed suppression of the secondary flow particularly the HV with the presence of the VG compared to without VG case.

Similarly, utilizing the knowledge gained in the fundamental study, VGs were used for thermal performance enhancement of pin fins which are usually employed in the heat transfer augmentation for internal cooling of the trailing part of a gas turbine blade/vane. Vortex generators were mounted in pairs upstream of the first row of in-line pin fins arrays. Thermal performance obtained numerically was compared without VGs and with VGs positioned at various locations with reference to the pin fins and yaw angles for various Reynolds numbers. The results illustrated that thermal performance was enhanced with VGs irrespective of the

VG angle and position compared to the case without VGs. However, the level of enhancement is dependent on the VGs angle and position. The VG placed at 45^{o} with a moderate gap between VGs and pin fins showed greater thermal performance.

In advanced gas turbines, the assembly of different components of the gas turbine may lead to some modifications in the flow paths. In an aero engine, when a low pressure turbine is connected to the nozzle section which has outlet guide vanes, a cavity is generated as a result of the assembly process. This cavity is formed upstream of an outlet guide vane. Different streamwise distances between the cavity and outlet guide vane (in this study an airfoil is considered) were investigated experimentally as well as numerically. Results demonstrated that the cavity located at a small distance is favorable as it considerably reduced the endwall heat transfer in the junction region of the airfoil. Similarly, the meeting parts of combustor and turbine are assembled via an axisymmetric contouring to match the diameters of both parts. So the effect of an axisymmetric endwall contouring on film cooling/heat transfer and secondary losses was numerically investigated for a nozzle guide vane (NGV) in a single passage region. It was revealed that an axisymmetric contouring enhanced the film cooling effectiveness. The heat transfer increased with the addition of film cooling which is obvious but the level of enhancement degraded with endwall contouring. Flow structures highlighted the suppression of the secondary flow.

Keywords: heat transfer, obstacle, vortex generator, pin fins, endwall, Nusselt number, thermal performance, film cooling effectiveness, contouring.

Acknowledgments

This research work has been carried out at the Division of Heat Transfer, Department of Energy Sciences, Faculty of Engineering (LTH), Lund University, Sweden. Accomplishment of this work is indeed a great blessing of Almighty.

I am sincerely thankful to my supervisor, Senior Professor Emeritus Bengt Sundén. He provided me opportunity to work with him by accepting me as a PhD scholar under his supervision. It was not possible for me to come to the level where I am now without his continuous supervision and guidance. His valuable direction and stress-free environment throughout my PhD study will ever be remembered. I would like to express my gratitude to my co-supervisor Dr. Lei Wang as well. Dr. Zan Wu cannot be ignored at this occasion without saying thanks to him.

I would also give my thanks to all the staff members and colleagues of our department, especially my PhD colleague Jian Liu. We worked together and I got a lot of help from him. Last but not the least I must say special thanks to my wife, whose support and encouragement have always been with me.

For financial support, I acknowledge the Higher Education Commission of Pakistan (HEC) and Swedish Research Council (VR). The travel grant from Royal Physiographic Society of Lund for attending a conference is also acknowledged.

List of Publications

Publications included in the thesis:

i. **Safeer Hussain**, Jian Liu, Lei Wang, Bengt Sundén, "Effects on endwall heat transfer by a winglet vortex generator pair mounted upstream of a cylinder", *Journal of Enhanced Heat Transfer*, 2016, Vol. 23, pp. 241-262.

ii. **Safeer Hussain**, Jian Liu, Lei Wang, Bengt Sundén, "Endwall heat transfer enhancement around cylinders with a wall-mounted vortex generator pair", *Proc. ASME International Mechanical Engineering Congress and Exposition*, November 3-9, 2017, Florida, USA, Paper No. IMECE 2017-70244.

iii. **Safeer Hussain**, Jian Liu, Lei Wang, Bengt Sundén, "Reduction of heat transfer on the endwall in the upstream junction region of a symmetric airfoil with vortex generator pair", *Proc. ASME Turbo Expo*, June 11-15, 2018, Oslo, Norway, Paper No. GT2018-75176.

iv. **Safeer Hussain**, Jian Liu, Lei Wang, Bengt Sundén, "Suppression of endwall heat transfer in the junction region with a symmetric airfoil by a vortex generator pair", *International Journal of Thermal Sciences*, 2019, Vol. 136 pp. 135-147.

v. Jian Liu, **Safeer Hussain**, Wei. Wang, Lei. Wang, G. Xie, Bent. Sundén, "Effect of the relative location of a pocket cavity on heat transfer and flow structures of the downstream endwall with a symmetrical vane", submitted for Journal publication.

vi. **Safeer Hussain**, Jian Liu, Lei Wang, Bengt Sundén, "Thermal performance enhancement in a wedge duct with in-line pin fins combined with vortex generators", *International Journal of Numerical Methods for Heat and Fluid Flow* (accepted).

vii. **Safeer Hussain**, Jian Liu, Bengt Sundén, "Study of effects of axisymmetric endwall contouring on film cooling and heat transfer in a cascade of first stage nozzle guide vane", submitted for Journal publication.

Author contribution

For all papers except one, the thesis author was responsible for developing the computational mode, performing simulations, validating the model against experimental data, carrying out experiments and analyzing the results as well as writing the draft papers. However, the experiments were carried out in close cooperation with another PhD student (mostly the second author). The co-authors assisted in planning, analysis and discussion and the main supervisor contributed significantly to the revision of the papers.

Publications not included in the thesis:

i. **S. Hussain**, B. Sundén, J. Liu, L. Wang, M. Andersson, "Experimental investigation of endwall heat transfer upstream of an obstacle in presence of vortex generator", *Proc. 9th World Conference on Experimental Heat Transfer, Fluid Mechanics and Thermodynamics* (ExHFT-9), June 12-15, 2017, Iguazu Falls, Brazil, paper No. 19.

ii. **S. Hussain**, J. Liu, L. Wang, B. Sundén, "Experimental investigation of heat transfer enhancement on the endwall around an obstacle embedded with a vortex generator pair", *Proc. International Heat Transfer Conference* IHCT-16, August 10-15, 2018, Beijing, Paper No. IHTC16-22151.

iii. J. Liu, **S. Hussain**, L. Wang, G. Xie, B. Sundén, "Heat transfer and turbulent flow characteristics over pocket cavity in the junction part of an outlet guide vane in a gas turbine", *Applied Thermal Engineering*, 2017, Vol. 124, pp. 831-843.

iv. J. Liu, **S. Hussain**, L. Wang, G. Xie, B. Sundén, "The effects of the pocket on heat transfer of endwall with a bluff body in the rear part of gas turbine", *Proc. ASME Turbo Expo*, 2017, June 26-30, 2017, Charlotte, USA, Paper No. GT2017-63191.

v. J. Liu, **S. Hussain**, L. Wang, G. Xie, B. Sundén, "Experimental and numerical investigations of heat transfer and turbulent flow in a rectangular channel mounted with perforated ribs", submitted for Journal publication.

vi. J. Liu, **S. Hussain**, W. Du, L. Wang, B. Sundén, "Arrangements of film cooling holes in the leading edge of a nozzle guide vane", submitted for Journal publication.

vii. J. Liu, **S. Hussain**, W. Wang, L. Wang, G. Xie, B. Sundén, "Heat transfer enhancement and turbulent flow in a rectangular channel using perforated ribs with inclined holes", *ASME Journal of Heat Transfer*, 2019, Vol. 141, paper No. 041702.

viii. J. Liu, **S. Hussain**, L. Wang, G. Xie, B. Sundén, "Effects of a pocket cavity on heat transfer and flow characteristics of the endwall with a bluff body in a gas turbine engine", *Applied Thermal Engineering*, 2018, Vol. 143 pp. 935-946.

ix. J. Liu, **S. Hussain**, C. Wang, L. Wang, G. Xie, B. Sundén, "Effects of the pocket cavity on heat transfer and fluid flow of the downstream outlet guide vane at different flow attacking angles", *Numerical Heat Transfer, Part A: Applications*, 2018, Vol. 74 pp. 1087-1104.

x. J. Liu, **S. Hussain**, J. Wang, L. Wang, G. Xie, B. Sundén, "Application of fractal theory in the arrangement of truncated ribs in a rectangular cooling channel (4:1) of a turbine blade", *Applied Thermal Engineering*, 2018, Vol. 139 pp. 488-505.

xi. J. Liu, **S. Hussain**, J. Wang, L. Wang, G. Xie, B. Sundén, "Heat transfer enhancement and turbulent flow in a high aspect ratio channel (4:1) with ribs of various truncation types and arrangements", *International Journal of Thermal Sciences*, 2018, Vol. 123 pp. 99-116.

xii. J. Liu, **S. Hussain**, L. Wang, G. Xie, B. Sundén, "Heat transfer and turbulent flow characteristics over pocket cavity in the junction part of an outlet guide vane in a gas turbine", *Applied Thermal Engineering*, 2017, Vol. 124 pp. 831-843.

Nomenclature

A	heater surface area (m^2)
C	nozzle guide vane chord length (m)
C_p	pressure coefficient
d	diameter (mm)
D_h	channel hydraulic diameter (mm)
f	friction factor
f_o	friction factor for smooth channel
H	height (mm)
h	heat transfer coefficient ($W/m^2 \cdot K$)
I	current (A)
k	thermal conductivity (W/m.K)
L	characteristic length scale (m)
l	distance between pressure points (m)
Nu	Nusselt number
Nu_o	smooth channel Nusselt number
$\overline{Nu}$	streamwise/spanwise averaged Nusselt number
$\overline{\overline{Nu}}$	area averaged Nusselt number
P	pitch of vane cascade (mm)
Pr	Prandtl number
q_c	convective heat flux (W/m2)
Q_{el}	heat generated by the electric heater (W)
Q_{rad}	heat loss by radiation (W)
Re	Reynolds number
S	span of NGV (mm)
S_x	normalized streamwise parameter
S_z	normalized spanwise parameter
T_{aw}	adiabatic wall temperature (K)
T_c	coolant temperature (K)
T_{lc}	liquid crystal temperature (K)
T_o	room temperature (K)
T_∞	mainstream fluid temperature (K)
TP	thermal performance
U_{max}	channel maximum velocity (m/s)
U_o	channel bulk velocity (m/s)
V	voltage (V)
X	streamwise distance between VG and cylinder
Z	spanwise distance between VGs

Greek symbols

α	angle of attack (degree)
Δp	pressure drop (Pa)
η	film cooling effectiveness
$\bar{\eta}$	streamwise/spanwise averaged film cooling effectiveness
$\bar{\bar{\eta}}$	area averaged film cooling effectiveness
υ	kinematic viscosity (m^2/s)
ρ	density (kg/m^3)

Abbreviations

CFI	counter flow inward
CFO	counter flow outward
CV	corner vortex
HV	horseshoe vortex
LC	liquid crystal
*NG*V	nozzle guide vane
*OG*V	outlet guide vane
PS	pressure side
SS	suction side
SV	secondary vortex
TBC	thermal barrier coating
TIT	turbine inlet temperature
TV	tertiary vortex
VG	vortex generator

Table of Contents

CHAPTER 1

Introduction

1.1 Motivation

Gas turbines are typically used in electricity production, aviation, marine and many more engineering applications. A lot of progress has been made on gas turbines due to their applications in industry. A modern gas turbine engine for aerospace is shown in Fig. 1.1. The most outstanding feature of a gas turbine is its efficiency. This is so as the enhancement of a gas turbine efficiency is linked to multifold benefits. The foremost advantage of enhanced gas turbine efficiency is the reduction in consumption of fossil fuels which are depleting with time fastly. The amount of reduction of fuel with the increase of efficiency can be estimated by considering a small increase of only 1% of the thermal efficiency for a 50MW gas turbine will give a potential to save approximately 750 tons/year of fuel [1]. The use of less fuel yields less amount of greenhouse gases and emissions leaving a positive impact on the environment of this planet which is tremendously important. According to the thermodynamic cycle [2], the straight away method to improve the gas turbine efficiency is to raise the gas turbine inlet temperature (TIT). In addition, for gas turbines with thrust generating devices like an aero engine (Fig. 1.1), the thrust is also proportional to TIT. Figure 1.2 shows the efficiency evolutions of different generations of gas turbines with the turbine inlet temperature. Similarly, controlling the losses occurring in gas turbines reduce the compressor work load and hence increases the work output of the gas turbine.

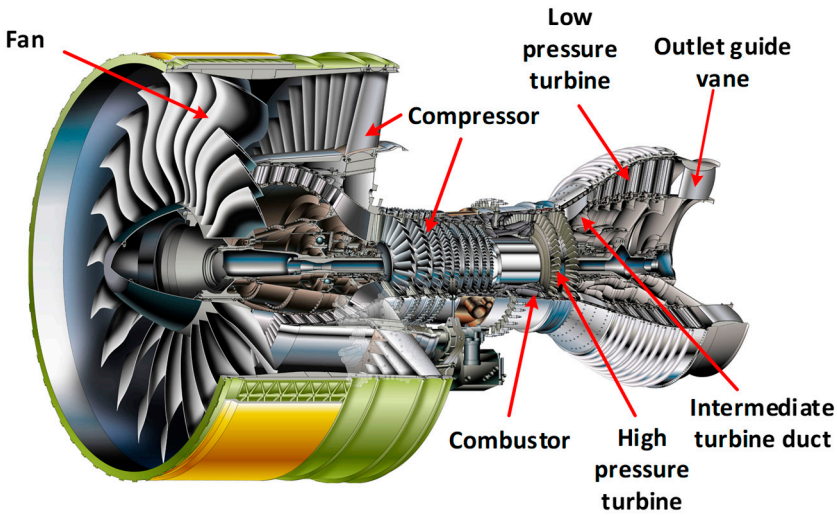

Figure 1.1: Cut view of a gas turbine, GP7200 aero engine [3].

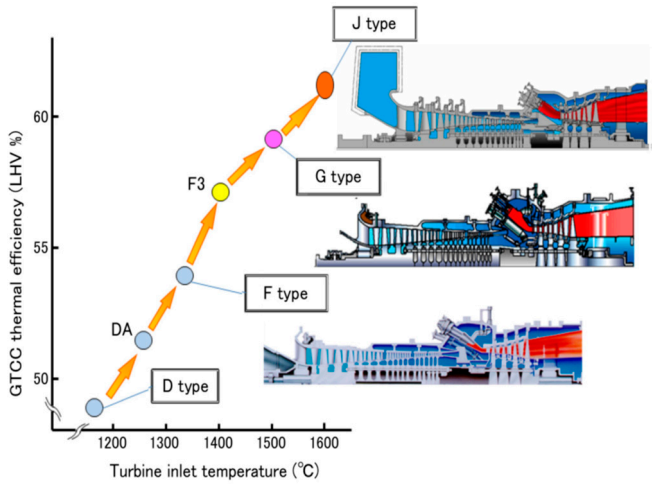

Figure 1.2: Gas turbine efficiency vs turbine inlet temperature [4].

The high TIT can be achieved with the use of state-of-the-art super alloys which can withstand high temperature but this is not the only option instead a small fraction of increase has been made possible due to the advanced material or use of thermal barrier coating (TBC) as today's modern gas turbines operate well above the allowable limit of these advanced materials. This has been made possible with super-efficient cooling. As illustrated in Fig. 1.3, a large

contribution for promoting the gas turbine inlet temperature is through advanced cooling. A part of the air from the compressor is deployed for cooling. So, an efficient cooling system can guarantee a further increase of the gas turbine inlet temperature and moreover, with a minimum amount of air as it imparts an extra load on the gas turbine.

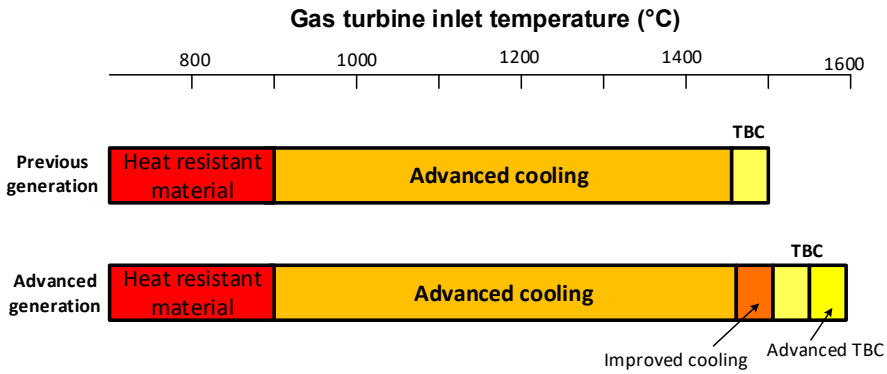

Figure 1.3: Role of cooling for raising the gas turbine inlet temperature (TIT), reproduced from [4].

In advanced generation gas turbines, the radial temperature profile is quite flat compared to the previous generations due to stringent emission regulations as shown in Fig. 1.4. For the flat temperature profile, walls of a gas turbine are further exposed to the hot gases even for the same central flame temperature. Therefore, it becomes more challenging and demanding for the state-of-the-art cooling.

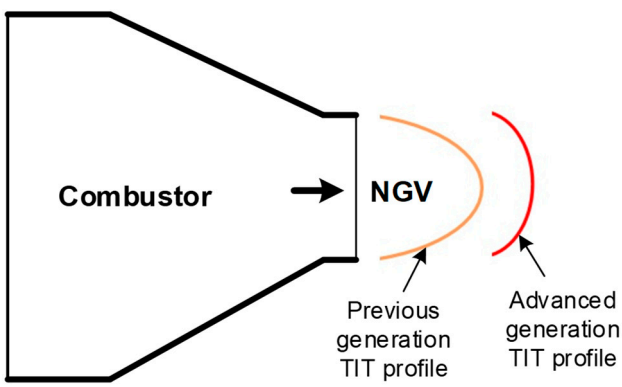

Figure 1.4: Schematic of radial temperature profile at combustor exit.

Gas turbine cooling can be classified into two types: i) internal cooling ii) external cooling. For internal cooling, the gas turbine blade/vane is divided into different channels and cooling air serpentines through these channels as shown in Fig. 1.5. Furthermore, different types of turbulence promotors (rib turbulators, pin fins etc.) are employed to enhance convective heat transfer. The flow losses are also increased due to these turbulence promotors so the best way is to achieve high heat transfer with minimum pressure losses collectively defined as thermal performance which is the major area of current research on internal cooling. Apart from pin fins and rib turbulators, a vortex generator (VG) is another boundary layer flow perturbating element extensively used in heat exchangers for heat transfer enhancement. The external cooling typically is called film cooling, in which cooling air ejects from a small hole (Fig. 1.5) and provides a protective layer between the metallic wall and hot gases. Film cooling is an essential part of cooling in advanced gas turbines.

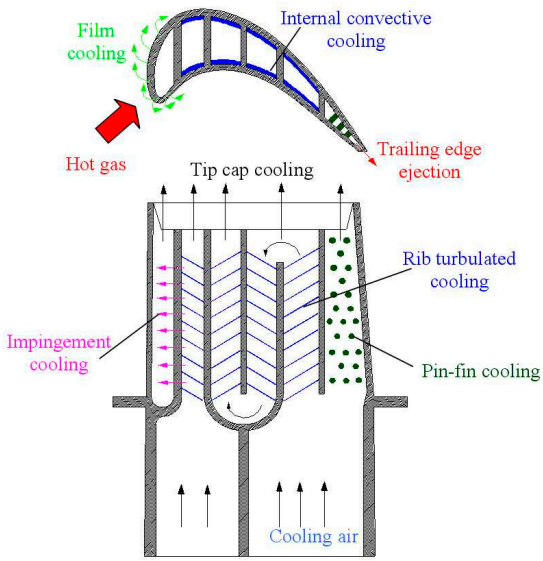

Figure 1.5: Gas turbine vane/blade cooling system.

A fluid approaching an obstacle placed in the flow encounters an adverse pressure gradient and starts to separate from the boundary and ultimately rolls up in the form of vortices giving secondary flow and causes pressure losses [5]. Such a situation arises in many ways in gas turbines, e.g., when flow passes through a gas turbine blade/vane and which acts as an obstacle and thus losses are induced. Typically, these type of losses are called secondary losses. Secondary losses play a crucial role in the performance and efficiency of a gas turbine [6]. Control of secondary losses can substantially boost gas turbine performance. Regarding heat transfer and secondary losses, the first stage nozzle guide vane (NGV) is very crucial because it faces extremely hot gases from the combustor and moreover having a small aspect ratio it has a high proportion of secondary losses.

1.2 Research Objectives and Methodologies

The aim of this research is to increase the heat transfer characteristics with minimum pressure drop and mitigate the secondary losses in order to enhance the gas turbine thermal efficiency. To achieve this goal, a relatively new flow perturbating element in gas turbine heat transfer enhancement, i.e., a vortex generator has been considered although it is commonly used in other applications like heat exchangers. It is widely used in the aerospace industry for triggering a prior onset of transition from laminar to turbulent boundary layer. The vortex generator is typically embedded in a boundary layer and it disturbs the boundary layer by generating vortices. On the other hand, vortices are also associated with an obstacle which appears in various parts of gas turbine components like vane/blade, support studs in the intermediate turbine duct (ITD) between high pressure (HPT) and low pressure turbine (LPT) and pin fins in the rear part of gas turbine blades for internal cooling.

In this study, with an idea of how the vortices accompanied by the obstacle and vortex generator interact with each other and what are their consequences on endwall heat transfer and pressure loss have been investigated. Initially, as a fundamental study, a flow approaching an obstacle was disturbed by installing a pair of vortex generators in the upstream of the obstacle. Following the fundamental study, the use of vortex generators was expanded to more actual application in pin fins cooling. In the latter investigations, use of the VG pair in the upstream of an airfoil representing a vane was investigated. Furthermore, the effect of a cavity upstream of an airfoil on the endwall heat transfer was studied. This cavity is formed as a result of the assembly of the outlet guide vane and last section of LPT. Finally, the first stage nozzle guide vane which is very crucial for the increase of gas turbine inlet temperature and hence thermal efficiency was investigated both for heat transfer and film cooling perspectives. In modern gas turbines, the connecting parts of the combustor and gas turbine (first stage nozzle guide vane) do not match. So usually these components are coupled via an axisymmetric contouring. The contouring affects the leading edge junction region of the first stage nozzle guide vane (NGV) in terms of heat transfer/film cooling and secondary losses.

The following major objectives were set up in this study:

- Perform a fundamental study, investigation of endwall heat transfer around an obstacle in the presence of a VG pair to find an optimal position of the VG.
- Implementation of the results obtained from the fundamental study into various components of the gas turbine.
- Investigation of heat transfer characteristics for situations arising in the assembly process of advanced gas turbines.
    - Study the effects of pocket cavity upstream of an outlet guide vane on the endwall heat transfer.

- Investigate the effect of axisymmetric endwall contouring on the performance of film cooling/heat transfer characteristics and secondary flow in a cascade of first stage nozzle guide vane.

To achieve these objectives, both experimental and numerical techniques have been employed. For experiments, liquid crystal thermography, a non-intrusive technique for temperature measurement, was employed whereas, state-of-the-art commercial software FLUENT was used for the numerical studies. For most of the numerical study, steady state Reynolds-averaged Navier-Stokes (RANS) equations were adopted with appropriate turbulence models depending on the applications.

1.3 Outline of the Thesis

The first chapter is comprised of an introduction which presenting the motivation behind the present study followed by research objectives and methodologies. Chapter 2 covers some fundamental aspects and literature review related to gas turbine components regarding heat transfer. It starts from some fundamental concepts and then moves to more complex and real gas turbine phenomenon. The experimental facility, experimental procedure and numerical approaches are explained in chapter 3. The results obtained from the experiments and numerical simulations are discussed in chapter 4. The results from each type of study are discussed in a separate section. Main findings from the present investigations are enclosed in chapter 5 and finally in chapter 6 some potential studies for the future are suggested as an extension to the present study.

CHAPTER 2

Fundamental Aspects and Literature Review

2.1 Role of Obstacle in a Flow

The study of effects of obstacles in a fluid flow is one of the oldest and imperative domain of studies since it has tremendous engineering applications. With pertinent to the gas turbine, it either exists by design (vane/blade) or is installed purposely to gain some benefits like pin fins etc. The great importance of the obstacle in a flow is due to the three dimensional secondary flow generated in presence of an obstacle. When an obstacle is placed in the flow path of a fluid, due to the viscous nature of the fluid, the boundary layer flow approaching the obstacle starts to separate from the boundary as a result of adverse pressure gradient and the boundary layer turns into a reversed flow at a certain level of the adverse pressure gradient. Thus the boundary layer rolls up and hence triggers various kinds of vortices. Parisner and Smith [7] reported four type of vortices as shown in Fig. 2.1 as a horseshoe vortex (HV) followed by a corner vortex (CV) with a secondary vortex (SV) and a tertiary vortex (TV). As shown in Fig. 2.1 the most prominent and paramount vortex structure is the HV. The horseshoe vortex formed in the stagnation region of an obstacle is segregated into two parts surrounding the obstacle on both sides as illustrated in Figure 2.2. The horseshoe vortex plays a very crucial role in many engineering applications particularly in gas turbines, hence vastly studied in the past [5, 8-11]. Eckerline and Langston experimentally measured the formation and characteristics of a horseshoe vortex. With the aid of Particle Image Velocimetry (PIV), Sahin et al. [11] predicted various stagnation points resulting from the formation of the horseshoe vortex. Downstream of the obstacle, there is a low pressure wake region. Moreover,

if the obstacle height is not spanning the whole fluid domain height, some additional vortices are formed like tip vortices etc. (Fig 2.2) [12].

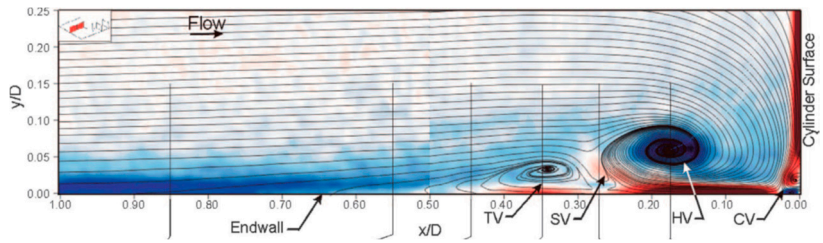

Figure 2.1: Vortices associated with an obstacle [7].

The secondary flow in the form of vortices associated with an obstacle, especially the HV, plays a very influential role in the heat transfer. The three dimensional vortical flow generated by the obstacle enhances the momentum exchange between the boundary layer and the main core flow and as a result heat transfer is enhanced and the level of enhanced heat transfer can reach 2-3 times [13, 14]. Beside benefitting heat transfer it also increases the pressure loss which is not desired in real applications. Due to its common use in applications, the flow features with an obstacle and associated heat transfer on the endwall as well as losses have been extensively studied by many researchers [15-19].

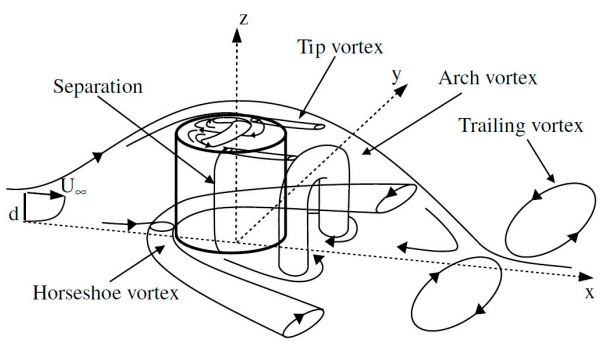

Figure 2.2: Schematic of vortices for a short cylinder [12].

Goldstein et al. [20] observed two high heat transfer peaks upstream of a square cylinder due to the vortical flow generated upstream of the obstacle in their investigations. Goldstein et al. [17] also studied the effect of heat transfer by the obstacle height to diameter ratio and showed that a short cylinder performs better in promoting the heat transfer downstream the obstacle. Similarly, Sparrow et al. [21] and Hinckel and Nagamatsu [22] experimentally reported enhanced endwall heat transfer with a circular cylinder for a range of Reynolds numbers. Later on, Yoo et al. [23] conducted an investigation to study the effect of the angle of attack of a cylinder of square cross section. They investigated the angle of attack from 0° to 45° and

found that the mass transfer peak in the vicinity of the obstacle was not significantly sensitive to the angle of attack. However, mass transfer was reduced due to the counter-rotating vortex with an increase of the angle of attack. Moreover, the local mass transfer from the square cylinder varied significantly with the angle of attack. Studying the shape of the obstacle, Chyu and Natarajan [24] investigated various geometrical shapes of the obstacles and observed that the strength of the HV greatly influenced the high heat transfer. Downstream the obstacles, the reattachment lengths for each geometrical shape were also measured and an obstacle with diamond shape showed the longest reattachment length. Similarly, Yan et al. [25] measured the heat transfer around cylindrical, diamond and square shaped obstacles by implementing the transient liquid crystal technique. Moreover, they also investigated the tandem effect of these obstacles by considering inline arrangements of two and three obstacles of the same geometrical shape. Wang et al. [26] also studied the tandem effect of obstacles on the endwall wall heat transfer as well as investigating a single obstacle. A numerical study conducted by Duchaine et al. [27] also investigated the endwall heat transfer with two square cylinders.

The high heat transfer associated with an obstacle has both positive and negative impacts in perspective of gas turbines and are described in the following sections.

2.2 Vortex Generator

A vortex generator as evident from its name is a small element that generate vortices when positioned in a flow. Like an obstacle, a vortex generator embedded in a boundary layer disrupt the boundary layer by generating vortices. The use of VG in aerodynamics for triggering the earlier transition from laminar to the turbulent boundary layer by interrupting the boundary layer is quite traditional. In addition to its use in aerodynamics, similar to an obstacle, the property of a VG generating vortices is beneficial for the enhancement of heat transfer and therefore widely used in heat transfer augmentation. Vortex generators are categorized owing to their shapes and types of vortices associated with them. These are wings and winglets vortex generators having rectangular or delta shapes [28]. However, winglet type vortex generators are superior compared to wing types and other shapes for heat transfer enhancement. [29]. Winglet type vortex generators are typically installed in pairs and generate pair of counter rotating vortices as depicted in Fig. 2.3. Moreover, a VG produces vortices either in longitudinal or spanwise direction thereby classified as longitudinal and spanwise vortex generator, respectively [30].

The flow characteristics and the vortices associated with VGs have been studied vastly in the past due to the widely use in engineering applications. Velete et al. [31] used a van-type vortex generator and obtained helical structures of vortices depending on the flow angle of the VG in an experimental study. On the other hand, You et al. [32] employed Large Eddy Simulations (LES) to numerically calculate the evolution of the vortical flow pattern in presence of a VG pair. They captured the flow toward or away from the endwall in the common region between the vortices depending on the orientation of the VG. Lu et al. [33] also discussed the vortices both experimentally and numerically. Similarly, velocity field and

other parameters related to momentum and heat transport near a VG were measured by Wroblewski and Eibeck [34]. Biswas and Chattopadhyay [35] studied the heat transfer enhancement for different Reynolds numbers with a delta shaped VG placed at various angles of attack. They reported spanwise averaged Nusselt number increase of 34 % at an angle of attack of 26^{o} even far downstream of the VGs. Gentry and Jacobi [36] also considered a delta wing and obtained the enhanced heat transfer characteristics using naphthalene sublimation technique. Moreover, using flow visualization techniques, some flow features were also captured. Some researchers like Wang et al. [37, 38] used vortex generators with impingement. They installed a pair of vortex generators upstream of an impingement jet hole. They varied the streamwise and spanwise positions of the VGs relative to the jet hole and measured the heat transfer in terms of Nusselt number. They also investigated rectangular and delta shapes of the VGs at various Reynolds numbers. Their study showed considerable enhancement of impingement heat transfer with VGs. Recently, Oneissi et al. [39] introduced new shapes of VGs, which they showed to provide more heat transfer augmentation than existing shapes.

Figure 2.3: Sketch of vortices generated by a pair of VGs [32].

2.3 Combined Obstacle and Vortex Generator

To meet the modern industry requirements, one needs more sophisticated and compact heat transfer devices. The intelligent approach to achieve this target is the hybrid use of these heat transfer augmentation devices. Ghorbani-Tari et al. [40-43] studied the combined effect of an obstacle and a rib on heat transfer. They employed a rib either upstream or downstream of an obstacle and reported considerable heat transfer enhancement. Vortex generators are extensively used in heat exchangers for heat transfer augmentation. In compact heat exchangers, tube bundles behave like obstacles and VGs are added to further promote the heat transfer thus making the heat exchanger more compact [44-47]. Biswas et al. [48] placed a pair of VGs on the rear side of a tube and numerically showed improved heat transfer in the wake region. Fiebig et al. [49] experimentally measured the heat transfer in a heat exchanger

with addition of VGs by employing liquid crystal thermography. Their study showed that the heat transfer was enhanced significantly with the installation of VGs for the inline configuration of the fins. Later on, Sinha et al. [50] used rectangular VGs and simulated cases with obstacles having in-line and staggered configurations. They studied the influence of the incidence angle of the VG pair on heat transfer. The incidence angle of attack of the VG was investigated by He et al. [51] at various Reynolds numbers and results presented a good heat transfer augmentation for VGs at an angle of 30^{o} and at low Reynolds number. Tang et al. [52] introduced a new shape of the vortex generator to enhance the heat transfer whereas, Lemouedda et al. [53] and Jang et al. [54] made an optimization study based on angle of attack and position of the VG. Recently, Gökçe [55] employed VGs for application in aerospace industry for internal cooling of gas turbine blades as well as external use to reduce the secondary losses.

2.3.1 Pin Fins

High endwall heat transfer with an obstacle is implemented in internal cooling of gas turbine blades in the trailing part. In the trailing part of a blade due to its geometric constraints, typically pin fins are employed to enhance the convective heat transfer. Pin fins are actually small obstacles arranged in the form of an array. Pin fins acting like obstacles interrupt the boundary layer due to the vortical and wake region flow phenomenon and as a result heat transfer is enhanced due to the additional mixing of the boundary layer and mainstream flow. Moreover, the secondary flow associated with one pin fin interacts with the neighboring pin fin and heat transfer is further enhanced. Pin fins are either arranged in staggered or in line fashion. The associated heat transfer and pressure drop with the pin fins depend significantly on the arrangement. In the investigation of Hwang et al. [56] staggered arrangement showed higher heat transfer than inline arrangement although pressure drop also increased. Lau et al. [57] reported quite different local mass transfer distributions with staggered and in-line arrangement of pin fins. On the other hand, Bianchini et al. [58] introduced a pentagonal arrangement for pin fins but heat transfer was not improved compared to pin fins arranged in staggered fashion. Similarly, the pin fin spacings in streamwise and spanwise directions are extremely important as this greatly affect the pressure drop hence degrade thermal performance. Lawson et al. [59] found that streamwise spacing plays a more significant role on heat transfer enhancement than the spanwise spacing, however, pressure drop showed opposite effect.

Other factors that influence the performance of pin fins are geometrical shape and size of the pin fins. Pin fins generally have height to diameter ratio of 0.5 to 4. Cylindrical shape of the pin fins is the most common shape used for pin fins. However, other shapes like square cross section have also been considered in many studies. Dabagh and Andrews [60] obtained the endwall and pin fin surface heat transfer contribution. They considered three different height-diameter ratio pin fins and showed that the wall or fin heat transfer was 15-35% higher than the pin surface heat transfer for all height to diameter ratios. Pin fins due to their high flow blockage impose huge pressure drop despite being good in heat transfer enhancement.

Therefore, for moderate heat transfer enhancement instead of pin fins, dimples or protrusions are used, which are relatively less expensive in terms of pressure loss. However, to add some additional heat transfer augmentation, dimples are accompanied with vortex generators [61, 62].

2.4 Vane Cascade

The high heat transfer upstream of an obstacle has negative impact in a gas turbine as well. Gas turbine vane/blade behaves like an obstacle and shoots the unnecessary endwall heat transfer in the upstream junction region [13, 63]. A junction region is formed between the gas turbine vane/blade and the wall on which the vane/blade is attached. The high heat transfer in the leading edge junction region of the blade/vane appears as a hot spot that can lead to failure or shortening the life of the gas turbine system and therefore, it must be addressed properly for the safe operation of a gas turbine. The HV generated in the stagnation region actually enhances the mixing of boundary layer flow with the main flow momentum in the near wall region and thus increases the heat transfer in the leading edge region largely [14, 63]. Similarly, the study of Luo et al. [64] also showed highly enhanced heat transfer in the junction region. Due to the high heat transfer in that region, the modern gas turbine with high TIT cannot be made possible for operation unless a protective layer is provided between the hub wall and hot combustion gases in the form of film cooling [65-68]. Particularly, the first stage nozzle guide vane which faces extreme thermal loading from the combustion gases needs special attention. Furthermore, the vortical flow originating in the stagnation region also spoils the film cooling in that region and therefore it becomes challenging to provide a sufficient protective coolant layer between the endwall and the hot gases. Additionally, the vortical flow in the junction region is the main source of secondary losses and this severity multiplies for the first stage NGV having small aspect ratio and it contributes as much as 30-50% of the total losses [6]. Moreover, in the cascade of NGV, the HV that originates in the upstream of the vane transforms into a complex vortical structure in the passage region of the cascade. The pressure side HV converts into the passage vortex and contributes greatly to the secondary losses Various models have been proposed for the secondary flow in the passage region in the literature [6, 69, 70] and one of the secondary flow models is illustrated in Fig. 2.4. Wang et al. [71] detected various shapes of the vortical structures at different locations in a cascade using smoke and laser beams and a proposed similar type of secondary flow model.

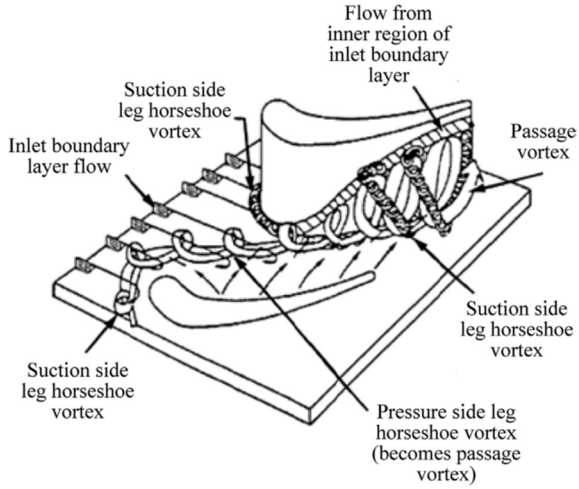

Figure 2.4: Model of secondary flow in a passage region [6].

Above discussion suggests that controlling the HV could be promising to lower the substantial heat transfer in the junction region as well as mitigating the secondary losses. Thus this gives two fold advantages. Many studies have been conducted in this manner to reduce the HV strength and consequently reduce the secondary losses and heat transfer. The most widely used method is to modify the leading edge region of the blade by fillets [72-75] and/or endwall contouring [76-79]. The study of Shih and Lin [73] employed leading edge fillet along with an inlet swirl and the results showed that both secondary losses and heat transfer (endwall heat transfer) were reduced by more than 30%. Moreover, endwall contouring is divided into two categories, i.e., non-axisymmetric and axisymmetric. The former is mainly employed for controlling the secondary losses while the latter will be addressed in the following section. In addition to mitigate the passage region losses, non- axisymmetric contouring also reduces the endwall heat transfer as shown by Saha and Acharya [80]. They considered a non-axisymmetric contoured endwall and revealed that local heat transfer in the junction region was reduced upto 25% whereas the overall reduction was 8% with a mass averaged pressure loss saving around 3%.

Another approach to suppress the HV and corresponding heat transfer/pressure losses is to use recirculating vortex flow [81]. A vortex generator formed by an air jet [82] and a forward facing step in the junction region were presented in [83]. The studies of Thrift et al. [84] and Takeishi et al. [85] revealed that the location of the film cooling hole in the junction region greatly affects the strength of the HV. These studies suggested that proper location of the film cooling hole in the junction region could suppress the HV strength.

In an aero engine, at the exit of the last stage low pressure turbine, a propeller/nozzle unit is attached which accelerates the air velocity to gain thrust. In the nozzle section of the aero engine outlet guide vanes (OGV) are used. The purpose of OGV is to straighten the flow leaving the low pressure turbine as it is swirled after passing through the blade passage

regions. Other than the aerodynamic use, an OGV also provides support structure for the rear part. The shape of the outlet guide vane is quite similar to a gas turbine vane and therefore flow characteristics upstream and within the passage region are similar. Wang et al. [86, 87] obtained high heat transfer upstream of an OGV in an experimental investigations similar to a gas turbine vane/blade. In modern aero engines, as the gas turbine part is connected with the rear part, a cavity is formed between the low pressure turbine and OGV. Due to the cavity formation, flow is disturbed and therefore it is critical to investigate it in terms of heat transfer on the endwall which has rarely been considered in the past.

2.4.1 Axisymmetric Endwall Contouring

In today's gas turbines there is a mismatch in dimensions between the combustor and the gas turbine joining parts. To enable the assembly of these two components, the diameters are matched by applying the axisymmetric contouring either on one or both walls. The axisymmetric contouring has been proven to reduce the unwanted junction region high heat transfer and secondary losses. In some of the past studies more attention was paid on the reduction of secondary losses whereas, others focused on heat transfer. A 20% loss reduction was reported by Barrigozzi et al. [88] with an axisymmetric contouring compared to the smooth endwall. The investigation with axisymmetric contouring conducted by Lynch et al. [89] displayed an overall 20% reduction of heat transfer as a result of reduced passage vortex strength. The past studies revealed that film cooling is also influenced by axisymmetric endwall contouring as investigated in the study of Barrigozzi et al. [90]. Shin et al. [78] employed two different types of contouring on the endwall and investigated the film cooling performance for a slot. The results showed improved film cooling effectiveness due to reduction of the vortical flow.

Moreover, while interfacing the combustor and gas turbine, a slot is retained deliberately upstream of first stage NGV to accommodate the thermal stresses and typically coolant air is passed through the slot as a leakage flow called slot cooling. The coolant from the leakage also contributes in generation of HV in addition to provide cooling. Lynch and Thole [91] experimentally studied nominal and reduced slot width (nominal slot width is reduced due to thermal expansion) and found that for the same mass flow rate, film cooling effectiveness was improved with the reduced slot. Thrift et al. [92] investigated the orientation and relative streamwise position of the slot. Slot orientation at 45^{o} showed better performance than 90^{o} and also formation of HV was affected by the orientation and position of the slot. Later on, Du et al. [93, 94] numerically investigated various parameters related to the slot .

CHAPTER 3

Experimental Methods and Numerical Approach

3.1 Temperature Measurement using Liquid Crystals

The traditional method for temperature measurement is using thermocouples. Being reliable, accurate and cheap, it is widely used in experiments. However, it is an intrusive method and can disturb the flow to some extent while using it for in-situ measurements. Moreover, a large number of thermocouples are required for regions of high temperature gradients to obtain the proper thermal profile as it only measures point-wise temperature. There are some alternative methods for temperature measurement like Infrared Thermography and Liquid Crystal Thermography (LCT) and others. These techniques are not only non-intrusive but also provide 2D temperature maps instead of point measurements. In contrast to thermocouples, the accuracy of these techniques strongly depend on calibration. An infrared camera is required for Infrared thermography, which is expensive, whereas an ordinary CCD camera is sufficient for LCT. Temperature measurement using liquid crystal thermography has been chosen for the experiments of this study.

A liquid crystal (LC) is a sheet consisting of polymeric material that contains a crystalline structure. Due to the crystalline nature of the structure, the white light that imparts on the liquid crystal sheet reflects the light of different wavelengths in various directions. The crystals are sensitive to temperature and change their orientation with a change in temperature. The change in orientation of the crystalline structure alters the light reflection property of the liquid sheet. Thus the liquid crystal sheet gives color change with a change in temperature by looking it at a certain view angle. Typically, at room temperature LC is transparent but due to

a black sheet at the bottom it appears as a black, with an increase in temperature its color starts changing from transparent to red, green and blue. There exist different kinds of LC sheets in the market with different specifications, i.e., various operating temperatures range with different bandwidths ranging from 0.5 ºC to 20 ºC. The liquid crystal technique is employed in two modes either in transient and steady state conditions. It is equally useful in transient mode due to its short response time (10-100 ms). In this study, steady state method has been implemented to obtain temperature contours.

3.2 Liquid Crystal Calibration

As the LC sheet changes color with temperature, calibration is required to know the color and temperature relation. The calibration is made either in-situ or before the experiments. However, in this study calibration has been achieved prior to the actual experiments. A calibration setup (Fig. 3.1) solely designed for LC sheet calibration by former students in the department has been used. It consists of a wooden box painted with black paint to avoid light reflection. A heater with a small fan was attached at the bottom of the front panel whereas, on the top rear side of the box there was an opening as an outlet to the airflow. The heater was attached with a transformer to control the power to the heater. At the center of the box, a small metallic plate with decent thermal conductive material like Aluminum was installed with a small holes drilled on it. A LC sheet was adhesively attached on one side of the metal plate whereas, thermocouples were inserted through the small holes on the other side of the plate. The LC sheets used here was from Hallcrest Ltd. with a specification of R35C5W which means that it has a bandwidth of 5 °C and red color starts at 35 °C. On the front panel of the box, a small Plexiglas window was inserted in front of the metal plate attached with LC sheet. A GigE Vision CCD camera with a resolution of 1600 1200 pixel was installed in front of the window with a specified view angle to record the images of the sheet during calibration measurements. Two white light sources (MASTER TL-D Super 80) were also placed on either side of the camera to illuminate the LC sheet uniformly whereas, the whole experimental setup with camera was covered with black cloth to avoid the background room light.

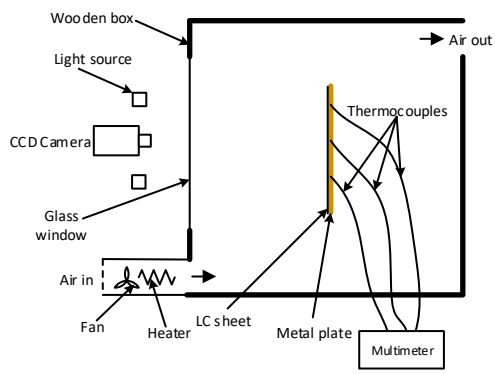

Figure 3.1: Schematic of the calibration set up.

To start the calibration experiment, initially the heater was switched on through the transformer while keeping the transformer power at low value. Meanwhile the fan was also started to make hot air to flow inside the wooden box. The steady state conditions indicated by the thermocouples were achieved after running the heater and fan for a few hours. Once steady sate condition was reached, image of the LC sheet was captured using the camera and stored on a Laptop that was attached to the camera. In the meantime, readings from the thermocouples were saved on the Laptop for a particular image and heater power. It is important to mention that temperature difference between the thermocouples was very small indicating the plate was uniformly heated. After making the first reading of the experiment, the power of the transformer was slightly raised. It should be noted that the increase in the heater power should not be too high as otherwise very few data points will be obtained. Keeping an eye on the thermocouples, when there was no change of temperature with time indicating the steady state condition at the new heater power. At this new heater power, the color of the sheet was also slightly changed from the previous reading. Another image of the sheet was captured followed by the thermocouples temperature recordings. Now heater power was further raised in a small amount and this process was continued until the color of the LC sheet was swapped from red, green and blue. To obtain the calibration at another view angle of the camera, the same procedure was repeated.

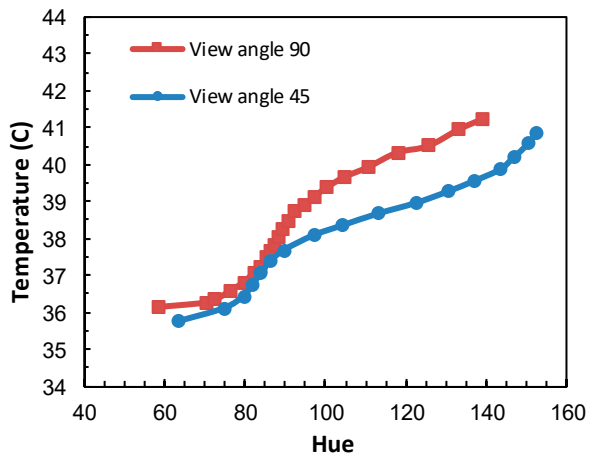

Figure 3.2: LC sheet calibration curves for 45^{o} and 90^{o} view angles.

Once all the images were obtained, then these images were imported and processed in MALTAB along with the corresponding temperature data from the thermocouples. The color information of these images in MATLAB was decoded into Hue, Saturation and Intensity (HIS). Selecting the central region of the image, an average Hue value was calculated for an image and similarly average temperature value was obtained from the thermocouples data for the corresponding image. Accordingly, one image and corresponding thermocouples data provided one data point and therefore, as many data points were obtained as the number of

images. These data points were plotted giving a calibration curve. The calibration curves for a view angle of 45º and 90º, respectively are shown in Fig. 3.2. Moreover, experiments for each view angle were repeated to get confidence on the calibration curve as it is very important for the accuracy of the experiments. The results showed that calibration curves for each view angle are repeatable. The complete range of hue values was not used in the actual experiments instead the hue values between 60-100 were used which represent green color. A similar calibration curve was also obtained by Wang [95] using the same calibration setup and procedure.

3.3 Test Facility

The test facility used for the experiments is comprised of an open suction type rectangular channel. The channel (Fig. 3.3) has a length of approximately 5 m and a cross section of 320 × 80 mm thus providing a hydraulic diameter (D_h) of 128 mm. The channel was made of Plexiglas transparent material with a wall thickness of 20 mm. The inlet of the channel was contoured to a bell shape mouth to provide a uniform flow at the inlet, whereas the other end of the channel was attached to a centrifugal fan which has a power rating of 3 kW. The air flow rate in the channel was controlled by controlling the frequency of the fan. A schematic of the test facility is shown in Fig. 3.4. As illustrated from Fig. 3.4, a segment approximately 500 mm of the channel was deliberately considered as the test section and is located at a distance of about 3.2 m from the inlet. The test section top wall is detachable to get access into it.

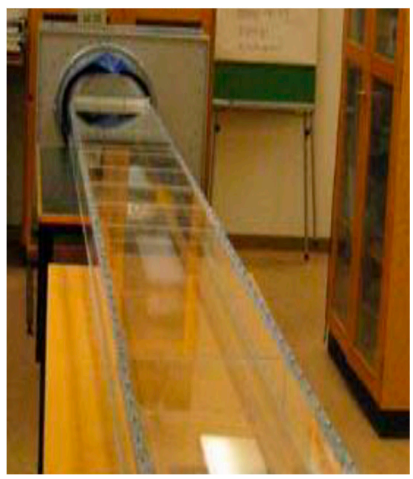

Figure 3.3: Snapshot of a long channel.

A foil heater made of Constantan (Copper-Nickel Alloy) covering the whole width (320 mm) of the test section bottom wall and having a length of 500 mm was adhered on the bottom of the test section. The heater was connected to an alternating current (AC) voltage source. A LC sheet from Hallcrest Ltd. with a brand name of R35C5W was carefully glued on the heater to avoid any void between the heater and the LC sheet. An object to investigate the effect on endwall heat transfer was installed above the LC sheet. The rear side of the test section was insulated with a 50 mm thick Styrofoam (low thermal conductive material) to minimize the heat loss by conduction. A CCD camera, same as used in the calibration experiment, was installed above the test section with a view angle of 90°. Moreover, to achieve the same conditions as those in the calibration experiment, the same two white light sources were placed on the either side of the camera for illuminating the LC sheet adequately. Two small holes were drilled on the upper wall of the channel upstream and downstream the test section to measure the pressure drop (ΔP) across the test section. Small plastic tubes with connectors were attached with these holes, whereas the other ends were connected to a manometer. Similar to the calibration experiment, the whole test section including the camera and light sources was covered with a black cloth to block the unnecessary light.

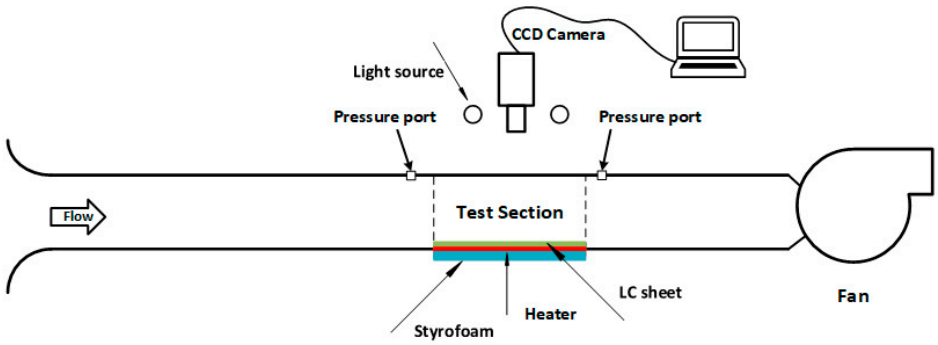

Figure 3.4: Schematic of the experimental setup.

3.4 Vortex Generator

The vortex generator used in this study is described as a delta winglet vortex generator shown in Fig. 3.5. The winglet type of VGs are typically employed in pairs, and therefore the same scheme was employed in this study. The height of the vortex generator was half the length throughout this study, however, different height of the VGs were used in different cases.

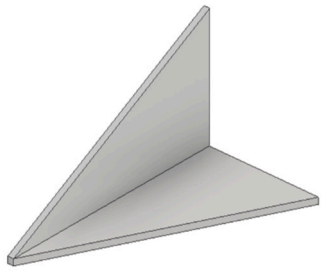

Figure 3.5: Geometry of the vortex generator.

3.5 Experimental Procedure and Measurement

Once the object to study the influence on the endwall heat transfer was installed in the test section, the centrifugal fan was switched on. The velocity of air in the channel was adjusted by the frequency regulator of the fan to obtain the desired channel bulk velocity (U_o). The velocity at the center of the channel, which is the channel maximum velocity (U_{max}), was measured by a Testo-416 anemometer. The maximum velocity(U_{max}) according to Schlichting [96] is related to the channel bulk velocity. Employing the channel bulk velocity (U_o), the required Reynolds number was obtained. After fixing the Reynolds number, the pressure was measured at two ports upstream and downstream of the test section using the pressure ports that are connected to the manometer through small plastic tubes.

Subsequently, power to the heater was applied in order to supply a constant heat flux on the endwall containing the LC sheet. This power should be adequate to change the liquid color slightly from the room condition (which is black due to the black paint). The heater should be continuously kept on the same power until the steady state condition was reached. Usually, it takes a few hours to get steady state. Once the steady state condition was achieved, an image of the specific region of interest of the test section was captured with the CCD camera and was stored in the computer. Meanwhile, for the particular image, the Voltage (V) and Current (I) from the multimeter and the room temperature from the thermocouple placed in the room was recorded and stored in the computer. After recording the first experimental measurement, the heat flux was increased by a small amount by increasing the heater power. Upon establishing the steady state again for the higher heat flux, a second measurement was made like the first one and this process was repeated until the green color was swapped through the whole region of interest as in the calibration curve hue values (60-100) corresponding to green color are chosen in these experiments. To come across the whole region of interest, about 20 images were captured but it varies from experiment to experiment. Each image has an information of surface temperature that belongs to a specific heat flux. Figure 3.6 shows a typical image of the liquid crystal for a certain heat flux with a VG pair and cylinder installed on the endwall. In this image only the green portion was utilized for the post processing, whereas, the rest of the image was disregarded.

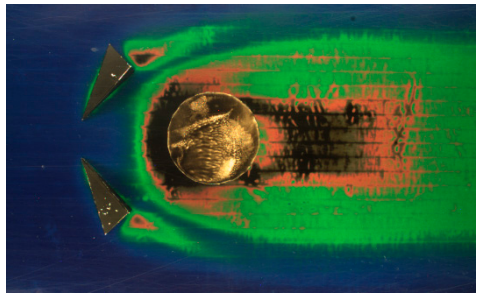

Figure 3.6: Snapshot of the endwall during experiments.

After accomplishing the experiments, the experimental data was processed in a MATLAB Code to obtain the LC sheet (endwall) surface temperature (T_{lc}). By knowing the endwall temperature (T_{lc}), the local forced convection heat transfer coefficient was calculated by Eq. (3.1)

$$h = \frac{q_c}{T_{lc} - T_0} \tag{3.1}$$

where, T_o is the room temperature measured by a digital thermometer. The room temperature is very close to the air temperature in the channel. Using the information of current (I) and voltage (V) collected during the experiments, the convective heat flux q_c was calculated using Eq. (3.2).

$$q_c = \frac{Q_{el} - Q_{rad}}{A} \tag{3.2}$$

where, A is the surface area of the heater, Q_{el} is the heat generated by the electric heater and Q_{rad} is the heat loss by radiation, while the heat loss due to conduction was not considered in this experiment as it is negligible, because the rear side of the test section was highly insulated. The convective heat transfer coefficient (h) is usually described in a non-dimensional form in terms of the Nusselt number (Nu). Equation (3.3) describes the Nusselt number definition used in this experiment.

$$Nu = \frac{hL}{k} \tag{3.3}$$

where k is the thermal conductivity of air and L is the characteristic length scale. The characteristic length scale (L) was different for different experiments and therefore has been specified in each set of experiments. Similarly, from the measured pressure drop, the friction factor was calculated using Eq. (3.4).

$$f = \frac{2D_h \Delta P}{l \rho U_o^2} \tag{3.4}$$

where, D_h is the hydraulic diameter of the test channel, l is the distance between pressure measuring ports and ρ is the density of air.

3.6 Cylindrical Obstacle and Vortex Generator

To investigate the coupling effect of vortices both from an obstacle and vortex generator on the endwall heat transfer, an obstacle with cylindrical cross section being most common in several applications was employed. The cylinder was vertically aligned in the test section of the channel on the LC sheet. The center of the cylinder was 300 mm downstream the leading edge of the test section. The cylinder height spans the whole height of the channel (80 mm). The origin of the coordinate system was at the center of the channel, with the x-axis in the streamwise direction, the z-axis in the spanwise direction and the y-axis is aligned with the vertical direction. A pair of delta winglet vortex generators was mounted on the bottom wall of the test section in front of the cylinder. A 3D view of the obstacle along with the VG pair in the test section is illustrated in Fig. 3.7. To investigate the orientation effect, the VG pair was installed in counter flow inward (CFI) and counter flow outward (CFO) orientations as demonstrated in Fig. 3.8. Referring to Fig. 3.8, the VGs make an angle of attack (α) with the *x*-axis. The streamwise distance between the obstacle and the VGs is (*X*) and the spanwise distance between the VGs is (*Z*). These were normalized by the cylinder diameter (*d*) and defined as S_x and S_z in Eq. (3.5) and Eq. (3.6), respectively. Further details are presented in **Paper i**.

$$S_x = X/d \tag{3.5}$$

$$S_z = Z/d \tag{3.6}$$

In order to find out the optimal location of the VGs and the angle of attack, Table 3.1 displays the values of the parameters S_x and S_z as well as attack angle (α) considered in the experiments. Moreover, these parameters have been investigated at Reynolds numbers from 20,000 to 50,000. The experimental procedure described in the preceding section was adopted for conducting the experiments and post processing of the experimental data.

Table 3.1. Parameters considered in the experiments.

Parameters	Values			
S_x	0.0	0.5	1.0	1.5
S_z	0.1	0.25	0.5	1.0
α	18°	30°	45°	-

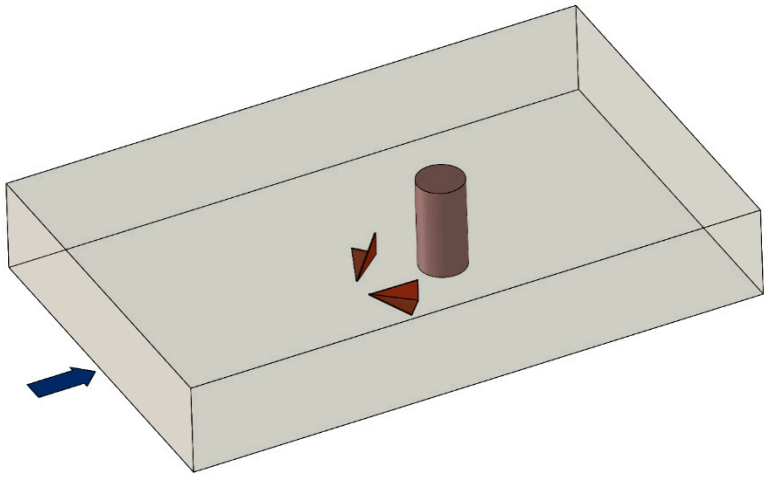

Figure 3.7: A 3-D view of the test section with cylinder and VG pair.

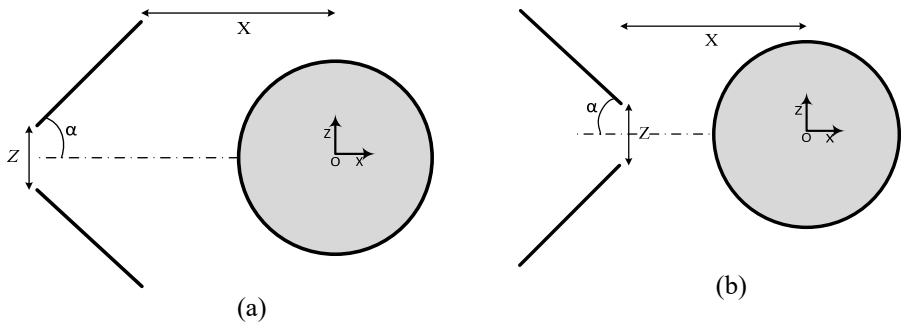

Figure 3.8: Relative positions of the VG pair upstream of the cylinder in (a) counter flow inward and (b) counter flow outward orientations.

3.6.1 Effect of Height to Diameter Ratio

The obstacle height in the channel plays a key role regarding the flow features and the associated endwall heat transfer. To study the effect of the obstacle height, the cylinder diameter was the same (40 mm) and the height of the cylinder was 40 mm and 80 mm (same as channel height) which offered height to diameter (*H/d*) ratios of 1 and 2, respectively. Learning from the preceeding experiments, the vortex generator pair was placed upstream of

the cylinder at a distance of 1d from the center of the cylinder in the counter flow inward (CFI) orientation with an angle of 45° as illustrated in Fig. 3.9 (**Paper ii**). The leading edges of the VGs were separated apart to 0.25d.

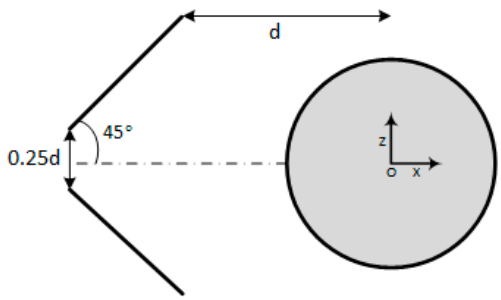

Figure 3.9: Layout of the VG pair with a cylinder.

3.6.2 Experimental Data Reduction

Four different Reynolds numbers ranging from 20,000 to 50,000 were investigated. The required Reynolds number (*Re*), defined in Eq. (3.7) based on the diameter of the obstacle, was achieved by controlling the frequency of the fan.

$$Re = U_0 d/\nu \tag{3.7}$$

where, d is the diameter of the cylinder. The Nusselt number was calculated by Eq. (3.8).

$$Nu = \frac{hd}{k} \tag{3.8}$$

The streamwise averaged Nusselt number was calculated as

$$\overline{Nu} = \frac{\int_{x/w=0.5}^{x/w=3.5} Nu(x,z)dx}{\int_{x/w=0.5}^{x/w=3.5} dx} \tag{3.9}$$

As installation of VGs in the flow impose some extra pressure drop, to quantify the actual advantage of the VG pair, a non-dimensional parameter called Thermal Performance (TP) was defined as

$$TP = \frac{\overline{Nu}/_{Nu_o}}{\left(f/_{f_o}\right)^{1/3}} \tag{3.11}$$

where, $\overline{\overline{Nu}}$ is the area averaged Nusselt number defined in Eq. (3.12).

$$\overline{\overline{Nu}} = \frac{\int_{\frac{x}{d}=-1}^{\frac{x}{d}=3.5}\int_{\frac{z}{d}=-1.7}^{\frac{z}{d}=1.7} Nu(x,z)dxdz}{\int_{\frac{x}{d}=-1}^{\frac{x}{d}=3.5}\int_{\frac{z}{d}=-1.7}^{\frac{z}{d}=1.7} dxdz} \tag{3.12}$$

where, Nu_o is the Nusselt number for a smooth channel that was obtained by the Dittus-Boelter correlation ($0.023Re^{0.8}Pr^{0.4}$) [97]. The Darcy friction factor (f) was calculated from the measured pressure drop using Eq. (3.4). The Darcy friction factor (f_o) for a smooth channel was calculated using the Blasius equation as

$$f_o = 0.316\left(\frac{U_o D_h}{\nu}\right)^{-0.25} \tag{3.13}$$

3.7 Axisymmetric Airfoil and Vortex Generator

Acquiring the detailed knowledge about the heat transfer modification on the endwall by the combination of bluff body and vortex generators from the previous experiments, it was revealed how the orientation and angle of attack of vortex generator can tailor the endwall heat transfer. This experiment was aimed to reduce the endwall heat transfer in the leading edge junction region of a blade/vane using vortex generators to avoid/reduce the hot spot in real gas turbines. Therefore, for simplicity instead of actual vane/blade, an axisymmetric airfoil was employed in these experiments along with vortex generators. An axisymmetric airfoil with circular leading edge diameter (d) of 40 mm and height the same as the channel height was installed in the test channel. For more details, refer to **Papers iii** and **iv**.

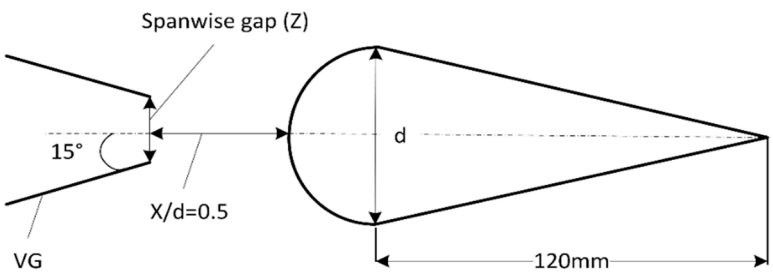

Figure 3.10: Layout of the VG pair upstream of an airfoil.

The vortex generator pair was embedded on the endwall at a streamwise distance of $x/d = 0.5$ from the leading edge of the airfoil, which is also origin (O) of the coordinate system making an angle of 15° with the x-axis as shown in Fig. 3.10. The spanwise gap between the VGs was varied as Z/d = 0.125, 0.25 and 0.5 for different cases. Moreover, two sizes of the VGs described as large VG and small VG dimensions as shown in Fig. 3.11 were utilized in this

study. A Reynolds number of 50,000 was obtained using Eq. (3.7) and Nusselt numbers (*Nu*) were calculated using Eq. (3.8) based on the leading edge diameter (*d*) of the axisymmetric airfoil. Furthermore, the streamwise averaged Nusselt number and area averaged Nusselt number were calculated using Eqs. (3.15) and (3.16), respectively.

$$\overline{Nu} = \frac{\int_{\frac{x}{d}=-0.5}^{\frac{x}{d}=0.5} Nu(x,z)dx}{\int_{\frac{x}{d}=-0.5}^{\frac{x}{d}=0.5} dx} \tag{3.15}$$

$$\overline{\overline{Nu}} = \frac{\int_{\frac{x}{d}=-0.5}^{\frac{x}{d}=0.5}\int_{\frac{x}{z}=-1.5}^{\frac{x}{z}=1.5} Nu(x,z)dxdz}{\int_{\frac{x}{d}=-0.5}^{\frac{x}{d}=0.5}\int_{\frac{x}{z}=-1.5}^{\frac{x}{z}=1.5} dxdz} \tag{3.16}$$

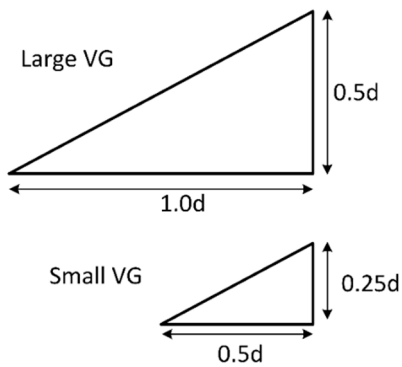

Figure 3.11:Dimensions of small and large VGs.

3.8 Axisymmetric Airfoil and Cavity

The pocket cavity is generated as a result of assembling the low pressure turbine and rear part of an advanced aero engine. There could be different shapes of cavity, but here a triangular shaped cavity was considered and instead of actual outlet guide vane, for easiness an axisymmetric airfoil was used and heat transfer on the endwall was measured experimentally. Numerical study was also performed to predict the heat transfer and flow structure under

strong recirculating flow generated within the cavity. An important parameter related to the cavity regarding heat transfer was investigated, i.e., the distance between the cavity and the airfoil. Three cases were studied with a cavity and one case without cavity (smooth endwall) at various Reynolds numbers. The cases with cavity were categorized on the streamwise distance between the airfoil and the trailing edge of cavity as shown in Fig. 3.12. Additional information can be found in **Paper v**. The geometry of the airfoil and cavity with dimensions is illustrated Fig. 3.12. It shows that the depth of the cavity is 50 mm and the airfoil was the same as used in the previous section.

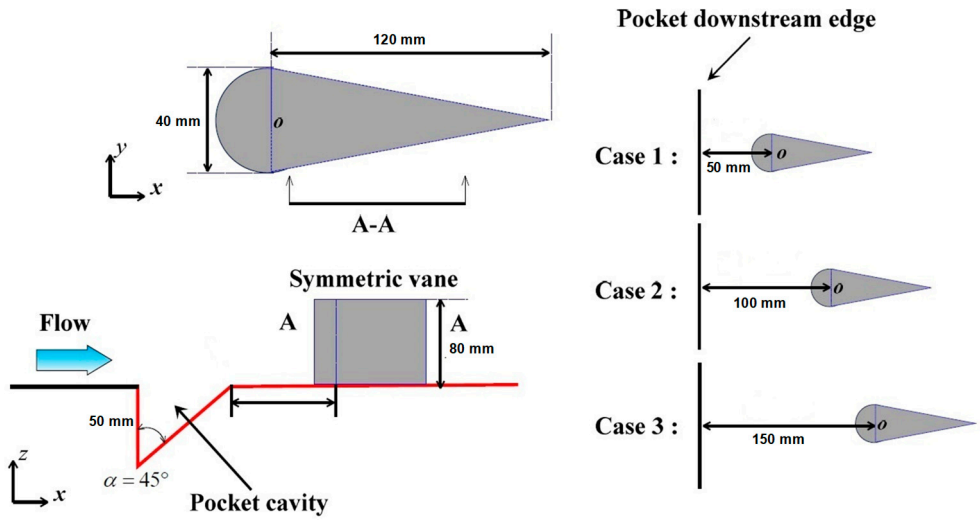

Figure 3.12: Configuration of pocket cavity and vane.

3.9 Pin Fins accompanied by Vortex Generators

After accomplishing the fundamental study on heat transfer with obstacle and VGs, a more practical approach for the internal cooling of the gas turbine trailing part was considered. In this study, numerical investigation of heat transfer in pin fins coupled with vortex generators was considered. The geometry and experimental conditions used were as those used in the experimental study by Hwang and Lui [98]. A wedge shape duct being more close to real applications was employed with 48 mm height at the inlet and it was reduced to 12 mm at the outlet whereas, both inlet and outlet were extended for numerical simulations as shown in Fig. 3.13. Pin fins with a diameter (d) of 12 mm were arranged in an in-line arrangements of five rows and height of the pin fins decreases as one moves from inlet to outlet because the channel was wedge shaped (Fig. 3.13). The streamwise and spanwise spacings between the pin fins were fixed as $S_x/d = S_y/d = 2.5$, which were found more appropriate according to previous studies and also adopted by Hwang and Lui [98]. Delta winglet vortex generators were installed in the form of pairs upstream of the first row of pins as illustrated in Fig. 3.14. The

shape of the VG was same as in Fig. 3.11 but the dimensions of the VG was smaller with height only equal to 0.5d and a length of 1d to avoid excessive pressure drop and mainly to disturb the boundary layer. Various cases were studied by varying the streamwise spacing (x/d=0.75, 1.0, 1.5) between VGs and pins and angle of attack of VGs 15°, 30° and 45° along with the base case (without VGs). The details are presented in **Paper vi**. Note that base case was the same as experimentally investigated by Hwang and Lui [98].

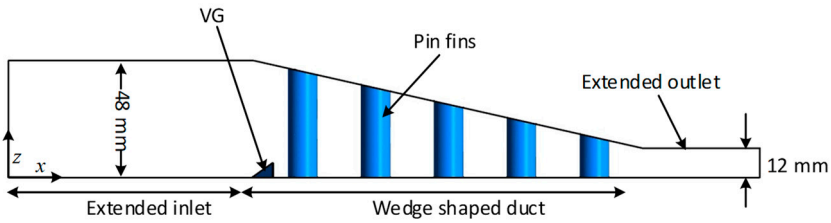

Figure 3.13: Computational domain for wedge shaped duct having pin fins and VGs.

The computational model was discretized with structured mesh having O-grid around the pins and Y-grid around VGs. The mesh near all the walls were established fine enough to achieve wall y^+ required by the SST $k-\omega$ turbulence model. The choice of SST $k-\omega$ turbulence model [99] was selected based on the previous studies similar to the present investigation [100, 101].

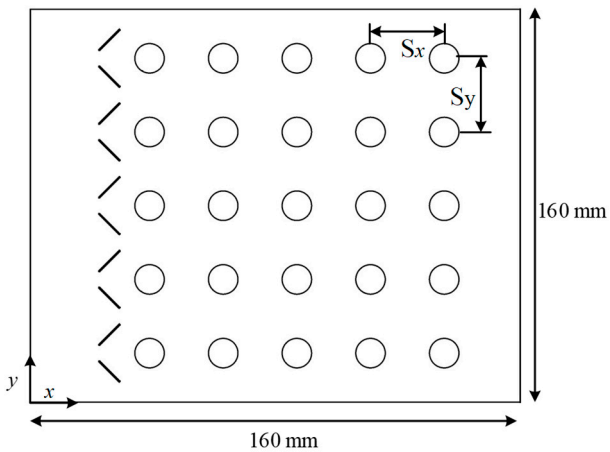

Figure 3.14: Pin fins and VGs pairs arrangement in test section.

A wide range of Reynolds number ($Re = U_o D_h/\nu$) from 10,000-50,000 was studied. The bulk velocity (U_o) at the inlet of the wedge duct was varied. The Nusselt number was defined as

$$Nu = \frac{hD_h}{k} \tag{3.17}$$

where, D_h is the hydraulic diameter of the duct at the inlet. Thermal performance was calculated as

$$TP = \frac{\overline{\overline{Nu}}/\overline{\overline{Nu}}_o}{\left(f/f_o\right)^{1/3}} \tag{3.18}$$

where, $\overline{\overline{Nu}}$ is area (wedge duct test section) averaged Nusselt number and f is the Darcy friction factor defined in Eq. (3.19) with pin fins and/or VGs

$$f = \frac{2D_h\Delta P}{l\rho U_o^2} \tag{3.19}$$

and $\overline{\overline{Nu}}_o$ and f_o is the area averaged Nusselt number and the Darcy friction factor, respectively for a smooth wedge duct without pin fins and VGs. The friction factors were based on the pressure drop calculated numerically across the wedge duct.

3.10 Axisymmetric Endwall Contouring

The axisymmetric endwall contouring was applied only on the inner wall in a cascade of a first stage nozzle guide vane. The contouring starts upstream of the NGV and ends at the leading edge of the NGV. The contoured segment was connected with the flat endwall through a radius (R) of 150 mm on both ends as shown in Fig. 3.15. The contouring angle (α) was varied as α = 0º,15º and 25º generating C_o, C_1 and C_2 cases, respectively (**Paper vii**). The NGV geometry and flow conditions were adopted as in the experiments by Sundaram and Thole [102]. In the junction region, 9 discrete film cooling holes with a diameter (d) of 4.6 mm were employed and a slot with leakage flow was placed at a distance of 17d from the stagnation point as shown in Fig. 3.16.

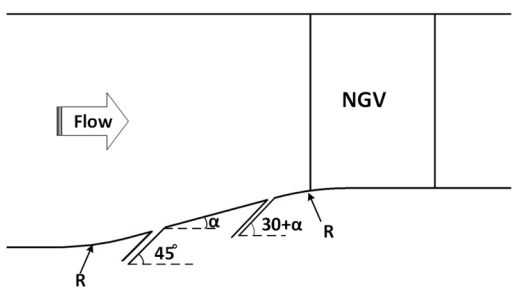

Figure 3.15: Layout of the contoured endwall with film and slot cooling.

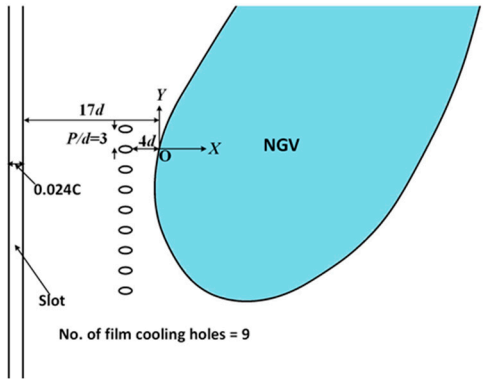

Figure 3.16: Arrangement of slot and film cooling holes.

The study was conducted numerically using ANSYS Fluent with a $k-\varepsilon$ based turbulence model. The selection of this turbulence model was based on previous similar studies, e.g., Wang et al. [68] and Hada and Thole [103]. In the family of $k-\varepsilon$ turbulence model, the Realizable $k-\varepsilon$ turbulence model was chosen with enhanced wall treatment was used. The computational domain consists of one passage region of NGV and shown in Fig. 3.17 together with the boundary conditions. The domain has two separated plenums for slot and film cooling.

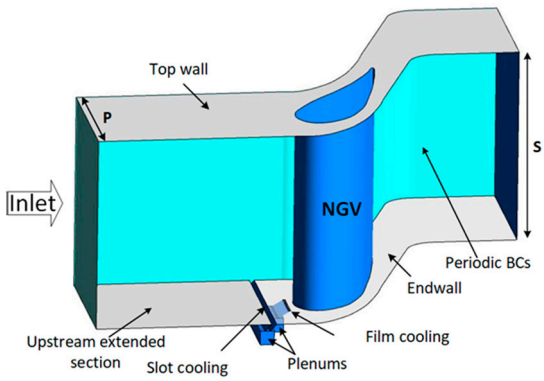

Figure 3.17: Computation domain illustrating boundary conditions.

The film cooling effectiveness and Nusselt number are defined in Eqs. (3.20) and (3.21), respectively.

$$\eta = \frac{T_\infty - T_{aw}}{T_o - T_c} \tag{3.20}$$

$$Nu = \frac{hC}{k} \tag{3.21}$$

where, T_∞ is the mainstream inlet temperature, T_{aw} is the adiabatic wall temperature and T_c is the coolant temperature. Moreover, h is the convective heat transfer coefficient and C is the NGV cord length.

3.11 Experimental Uncertainties Estimation

The uncertainties in the experimentally measured quantities were estimated using the method proposed by Moffat [104]. In general, according to Moffat [104], the uncertainty (δR) in an experimentally measured quantity R is a function of independent variables and is estimated by the root sum square method, mathematically expressed in Eq. (3.22)

$$\delta R = \left[\sum_{i=1}^{N} \left(\frac{\partial R}{\partial x_i}\delta x_i\right)^2\right]^{1/2} \tag{3.22}$$

where, $\frac{\partial R}{\partial x_i}$ is the sensitivity coefficient of R and δx_i is the uncertainty in variable x_i. Applying Eq. (3.22) for a specific quantity e.g., Nusselt number (Nu) is described as follows:

The Nusselt number is defined as

$$Nu = \frac{hd}{k} \tag{3.23}$$

Using the definition of convection coefficient (h) from Eq. (3.1), Eq. (3.23) takes the form

$$Nu = \frac{q_c d}{k(T_{lc} - T_o)} \tag{3.24}$$

The uncertainty in Nu using Eq. (3.22) can be written as

$$\delta Nu = \left[\sum_{i=1}^{N} \left(\frac{\partial Nu}{\partial x_i}\delta x_i\right)^2\right]^{1/2} \tag{3.26}$$

Employing Eq. (3.24) in Eq. (3.26), results in

$$\delta Nu = \left[\left(\frac{\partial Nu}{\partial q_c}\delta q_c\right)^2 + \left(\frac{\partial Nu}{\partial T_{lc}}\delta T_{lc}\right)^2 + \left(\frac{\partial Nu}{\partial T_o}\delta T_o\right)^2 + \left(\frac{\partial Nu}{\partial d}\delta d\right)^2 + \left(\frac{\partial Nu}{\partial k}\delta k\right)^2\right]^{1/2} \tag{3.27}$$

By considering $\delta d = \delta k = 0$, one finds

$$\delta Nu = \left[\left(\frac{\partial Nu}{\partial q_c}\delta q_c\right)^2 + \left(\frac{\partial Nu}{\partial T_{lc}}\delta T_{lc}\right)^2 + \left(\frac{\partial Nu}{\partial T_o}\delta T_o\right)^2\right]^{1/2} \tag{3.28}$$

Now from Eq. (3.24) the partial derivatives are

$$\frac{\partial Nu}{\partial q_c} = \frac{d}{k(T_{lc}-T_o)} \tag{3.29}$$

$$\frac{\partial Nu}{\partial T_{lc}} = \frac{-dq_c}{k(T_{lc}-T_o)^2} \tag{3.30}$$

$$\frac{\partial Nu}{\partial T_o} = \frac{dq_c}{k(T_{lc}-T_o)^2} \tag{3.31}$$

so Eq. (3.28) becomes

$$\delta Nu = \left[\left(\frac{d}{k(T_{lc}-T_o)}\delta q_c\right)^2 + \left(\frac{-dq_c}{k(T_{lc}-T_o)^2}\delta T_{lc}\right)^2 + \left(\frac{dq_c}{k(T_{lc}-T_o)^2}\delta T_o\right)^2\right]^{1/2} \tag{3.32}$$

rearranging above equation using Eq. (3.24)

$$\delta Nu = \left[\left(\frac{Nu}{q_c}\delta q_c\right)^2 + \left(\frac{Nu}{(T_{lc}-T_o)}\delta T_{lc}\right)^2 + \left(\frac{Nu}{(T_{lc}-T_o)}\delta T_o\right)^2\right]^{1/2} \tag{3.33}$$

or

$$\delta Nu = Nu\left[\left(\frac{\delta q_c}{q_c}\right)^2 + \left(\frac{\delta T_{lc}}{(T_{lc}-T_o)}\right)^2 + \left(\frac{\delta T_o}{(T_{lc}-T_o)}\right)^2\right]^{1/2} \tag{3.34}$$

or

$$\frac{\delta Nu}{Nu} = \left[\left(\frac{\delta q_c}{q_c}\right)^2 + \left(\frac{\delta T_{lc}}{(T_{lc}-T_o)}\right)^2 + \left(\frac{\delta T_o}{(T_{lc}-T_o)}\right)^2\right]^{1/2} \tag{3.35}$$

Equation (3.35) is the final form of the uncertainty in the Nusselt number (Nu). The uncertainty in the temperature measurement for T_{lc} and T_o was ± 0.2 K and ± 0.1 K, respectively. The uncertainty in the heat flux (q_c) was estimated to 4%. Based on these uncertainties, the uncertainty in Nusselt number (Nu) was calculated to ±8%.

Similarly, adopting the same procedure, the uncertainties for other quantities can be established. Variation in the friction factor was estimated to ±5% having an uncertainty in velocity and pressure drop of 2% and 3%, respectively.

CHAPTER 4

Results and Discussion

4.1 Validation of Test Facility

Before proceeding to the main results, it is essential to validate the experimental setup and procedure. In this regard, a smooth channel was considered, i.e., without any obstacle and vortex generator. Experiments were performed using the same method as was employed for the main experiments and contours of endwall Nusselt numbers were obtained. The experimentally calculated Nusselt numbers at the center line were normalized with the Dittus-Boelter correlation [97] and are shown in Fig. 4.1 for a Reynolds number of 96,000 based on the channel hydraulic diameter. The high Nusselt number in the beginning of the test section illustrated the undeveloped thermal region. The high heat transfer decayed in the streamwise direction and ultimately achieved the fully developed thermal state. In the fully developed thermal region, the experimentally calculated *Nu* achieved the theoretical value of the Nusselt number ($^{Nu}/_{Nu_o} \approx 1$) and thus validated the test section as well as the methodology of the experiments.

4.1.1 Test Section Characteristics

To characterize the test section, the velocity profile and turbulent intensity were measured experimentally. The velocity profile in the test section was determined using Particle Image Velocimetry (PIV). In this experiment Nd:YAG Lasers were used having a wavelength of 532 nm. The energy of the Laser was 120mJ per pulse. The time duration of the pulse of the Laser was about 10 ns and the maximum pulse frequency was 4Hz. Vegetable oil was used

to create the seeding particles and particles were generated by a six jet atomizer. A Nikon AF Micro 120f/2.8D camera with resolution of 1280×1024 pixels was employed. About 1000 images were recorded and using the software available with the PIV system, the velocity profile was found. It is important to mention that while obtaining the velocity profile, a cross correlation with a window of 64×64 pixels was adopted and the velocity profile is shown in Fig. 4.2. Due to practical limitations and the large window, cross correlation data points close to the wall are missing.

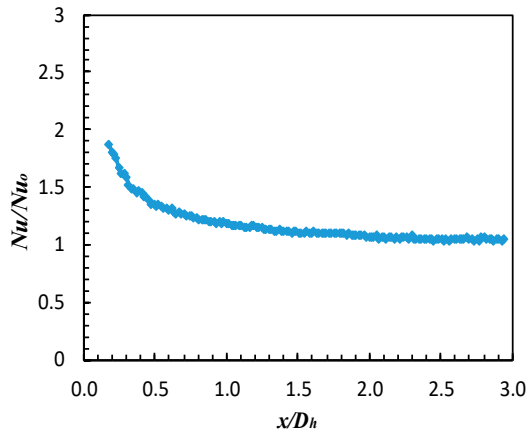

Figure 4.1: Normalized Nusselt number distribution at the center line of the smooth channel.

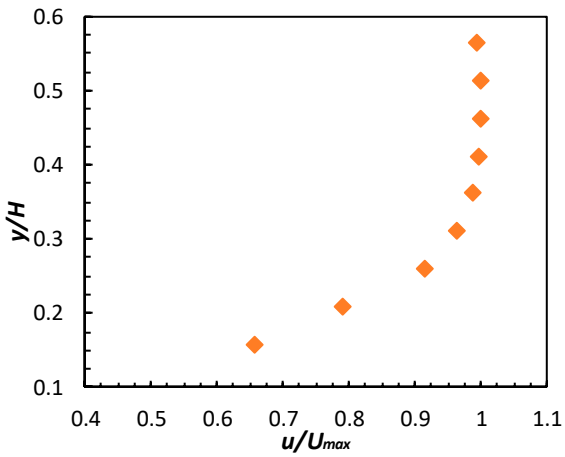

Figure 4.2:Measured velocity profile in the test section

Similarly, the turbulence intensity at the center of the channel was measured using hot wire anemometry. The hot wire (diameter = 5 μm) used was based on constant temperature wire made of Tungsten. The measured turbulence intensity was around 5% obtained with a sampling frequency of 1 kHz.

4.2 Cylindrical Obstacle and VG Pair

The complete set of results are presented in **Papers i and ii**.

4.2.1 Study of Angle of Attack and Orientation of the VG

The orientation of the VG induces down wash or up wash and this has an impact on the endwall heat transfer. Moreover, the strength of vortices generated by the vortex generator depends on the angle of attack of the VG. The position of the VGs was fixed at S_x = 1.0 and S_z = 0.5, whereas, orientation and angle of attack of the VG was varied. The Nusselt number contours are compared in Fig. 4.3 for VGs at an angle of attack of 18^o in counter flow inward (CFI) and counter flow outward (CFO) orientations with the base case at a Reynolds number of 30,000. The contours obtained at the angle of attack of 30^o and 45^o were omitted as patterns were the same. The Nusselt number contours revealed that the orientation of the VG pair plays a fundamental role for the endwall heat transfer. Interaction of the vortices generated by the VG pair and cylinder affected the endwall heat transfer in an opposite way greatly depending on the orientation of the VG pair. For the CFO configuration, the vortices generated from both elements interacted destructively and thus reduced the endwall heat transfer compared to the case without the VG pair, both upstream and downstream of the cylinder. The high heat transfer zone upstream the cylinder was considerably reduced in magnitude and its width was also reduced. Similarly, the high heat transfer region following the wake region downstream of the cylinder was also reduced in magnitude.

In contrast, for the VG pair placed in the CFI configuration, heat transfer was enhanced both upstream and downstream of the cylinder. This is a clear indication of strengthening of the horseshoe vortex by the induced vortices from the VG pair. The exchange of momentum from the hot fluid and the relatively cold fluid from the mainstream flow was increased as a result of the increased vorticity. The upstream high heat transfer band was increased in width as well as in magnitude. Similarly, in the downstream region, the high heat transfer region was wider and also increased in magnitude. However, the overall pattern of heat transfer is similar to the base case indicating that vortices generated by the obstacle are stronger than the vortices generated by the VG pair. In addition, there is a local high heat transfer spot in the immediate downstream region of each VG illustrating the strong vortices associated by the VGs and their dissipation in the downstream direction. The high heat transfer spot was more prominent for the CFO case than for the CFI case. Another important feature is that the heat transfer enhancement spread more in spanwise direction for the CFI orientation and remained consistent far downstream in the spanwise direction, whereas, for the CFO orientation it was squeezed with the streamwise distance downstream of the cylinder compared to the base case.

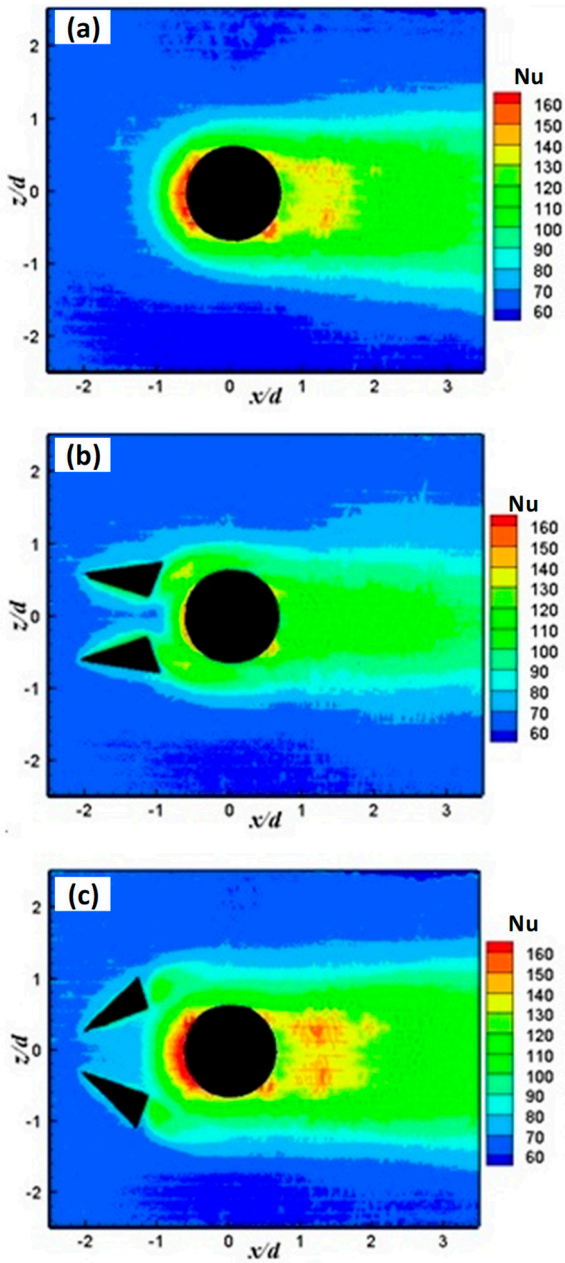

Figure 4.3: Nusselt number contours for (a) base case (b) VG pair in CFO orientation (c) VG pair in CFI orientation.

Figure 4.4 quantitatively analyzes the streamwise averaged Nusselt numbers ($\overline{Nu}$) by applying Eq. (3.9). This figure shows how the streamwise average Nusselt numbers differ from the base case at various spanwise positions. It is clear from the graphs that the central part is not very effective regarding the heat transfer enhancement. However, a reduction of heat transfer was found in that region for the CFO orientation. A substantial amount of heat transfer enhancement was depicted for the CFI orientation and it increased with the increase of the angle of attack. The level of heat transfer enhancement with VGs decreased in the spanwise direction and it approached the base case at $|z/d| = 1.7$ but for α = 45° it expanded even more. For α = 45° the pattern of the heat transfer was different from those of the other two lower angles. Two local maxima of heat transfer were found at the spanwise position where the vortex generators were located.

It is evident that increasing the angle of attack increases the strength of the longitudinal vortices. This indicates that a higher angle of attack augments the endwall heat transfer more. Nevertheless, increasing the angle of attack of the VG pair imposes higher pressure drop due to the increased projected area of the VGs. Therefore, the Thermal Performance (TP) described by Eq. (3.11) was used to find the effective heat transfer augmentation. As depicted in Fig. 4.5, TP increased with the angle of attack for both configurations. However, for the CFI configuration TP was always higher than that of the base case whereas, for the CFO it was lower than the base case except for α = 45° where it approached the base case. The findings in the graph revealed that the VG pair in the CFI configuration with α = 45° provided the best performance. Thus a VG pair with an attack angle of 45° having CFI configuration is more appropriate for the endwall heat transfer enhancement and a VG pair at low angle with CFO configuration is suitable for heat transfer reduction applications.

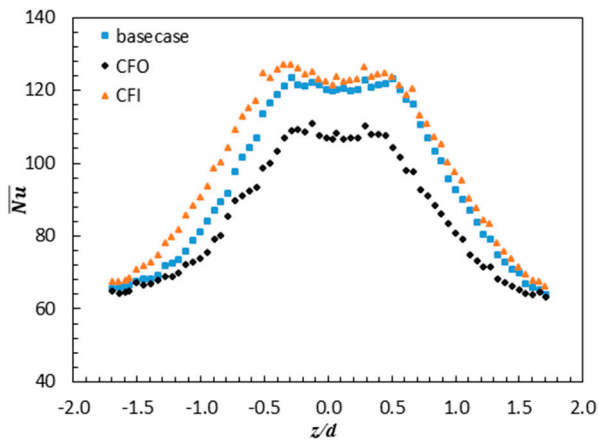

(a)

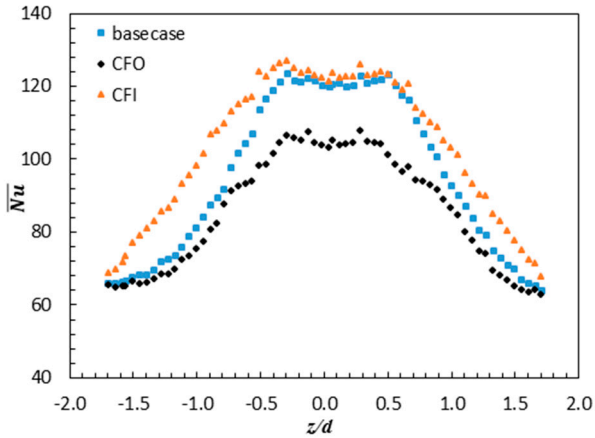

(b)

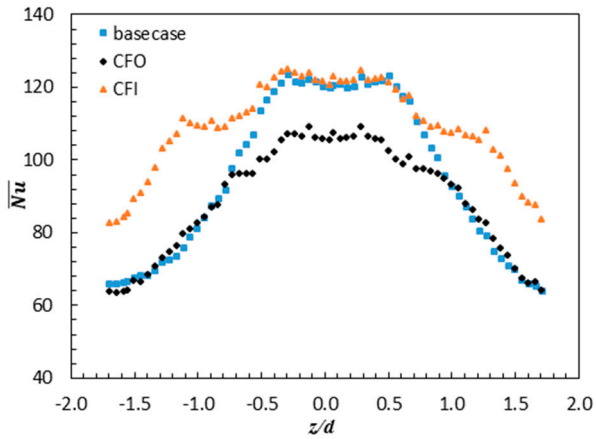

(c)

Figure 4.4: Streamwise averaged Nusselt numbers with VG at angle of attack of (a) 18° (b) 30° (c) 45°.

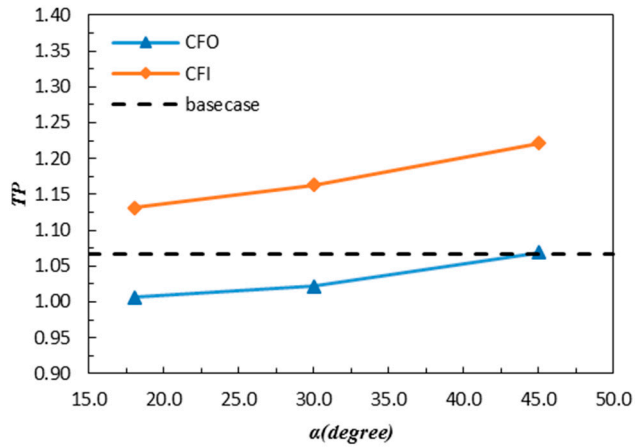

Figure 4.5: Thermal performance vs VG angle of attack.

4.2.2 Effect of Streamwise Variation of the VG Pair

After specifying the angle of attack and the orientation of the VG pair, the streamwise distance between the VG pair and the cylinder is another parameter that needs to be investigated. The angle of attack and the spanwise gap between the vortex generators were kept constant as 45^o and $S_z = 0.5$, respectively, whereas the streamwise distance was varied according to Table 3.1 from $S_x = 0$ to 1.5 with a step of 0.5. The Nusselt number contours for all the streamwise positions are displayed in Fig. 4.6. The shapes of the Nusselt number contours are all similar except for the case where the VG pair was very close to the obstacle ($S_x = 0$). In this case, the VG pair performed like a part of the obstacle and it appears like the shape of the obstacle was modified and consequently the heat transfer pattern was also changed. On the front side of the obstacle, it maintained the similarity with the base case but on both sides of the cylinder two high heat transfer streaks emerged due to the strong coupling effect of the vortices. Downstream the cylinder, the wake region was extended in both directions. As there is a small gap between the VGs and the cylinder, the flow velocity was accelerated and thus the wake region was extended. Similarly, the high heat transfer region following the wake region, formed an oval shape structure around the wake region and it covered a wide region. On the other hand, for the other three positions of the VG pair, the upstream high heat transfer region became broader in width and increased with an increase of S_x. However, the change in magnitude of Nu was not significant. It is also evident from the graphs that with the increase of the gap between the VG pair and the cylinder, there was a comparatively low heat transfer region between the vortex generator and the cylinder. This indicated that increasing the gap degraded coupling phenomenon of the vortices.

In the wake region immediately downstream of the cylinder, there was a decreasing trend of the wake region with an increase of S_x. It appeared similar to the base case (Fig. 4.3a) at S_x = 1.5. Again this indicated that a weak interaction of the horseshoe vortex with the longitudinal

vortex of the VG pair appeared as the axial distance between these objects was increased. The peak region adjacent to the wake region in the downstream region was also dependent on S_x. At S_x = 0.5, it was expanded in the spanwise direction, whereas for S_x = 1.0 it was squeezed and for S_x = 1.5 the peak value was increased compared to the other cases.

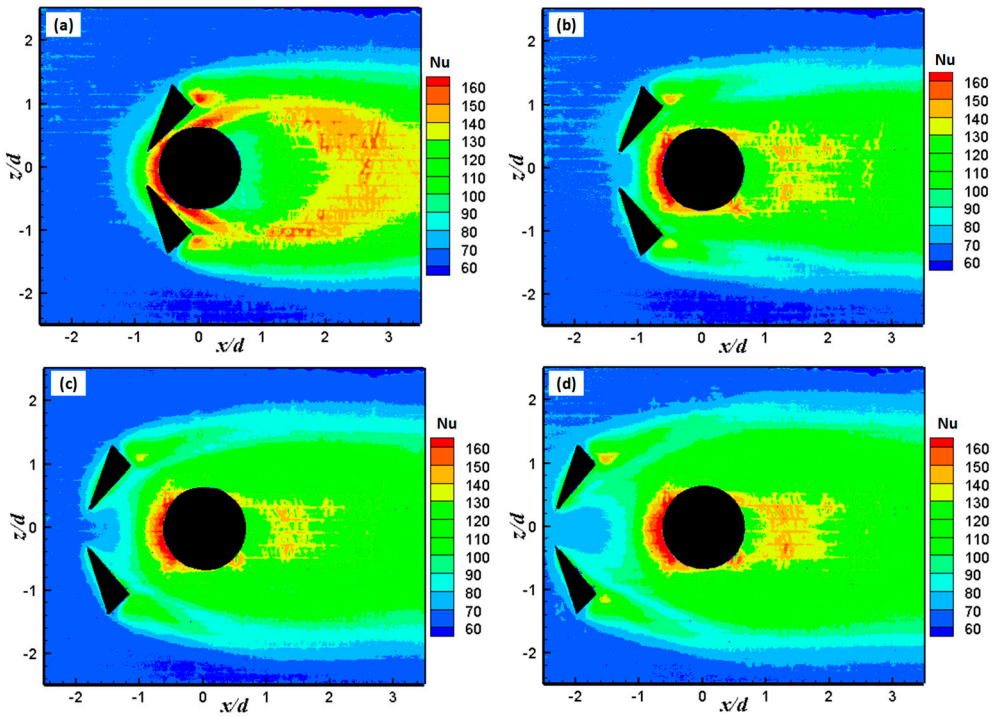

Figure 4.6: Nusselt number contours at *Re* = 30,000 with VG pair at streamwise positions of (a) S_x = 0 (b) S_x =0.5 (c) S_x =1.0 (d) S_x =1.5.

The thermal performance was also calculated for all the cases. As depicted in Fig. 4.7, TP was significantly enhanced with the addition of the VG upstream of a cylinder compared to the case of only a cylinder irrespective of the relative positions of the VG pair. However, the level of enhancement depends on the streamwise positions of the VGs relative to the obstacle. The thermal performance was highest at the nearest position of the VG and decreased at S_x = 0.5. Further increase of S_x did not change the TP significantly although a slight increase was observed at S_x = 1.5.

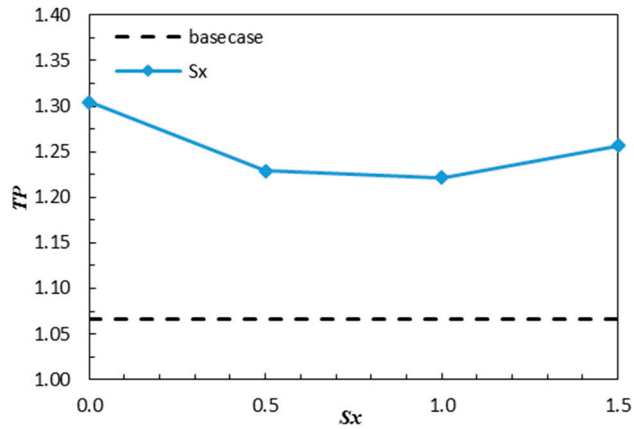

Figure 4.7: Thermal performance vs streamwise variation of the VG pair.

4.2.3 Spanwise Variation of the Gap of the VG Pair

It is equally important to study the spanwise gap between the VGs with an aim to identify the optimal gap between the VGs. The streamwise position was fixed as $S_x = 1.0$ having an angle of attack of 45°. The gap between the VGs according to Table 3.1 was varied from $S_z = 0.1$ to 1.0. The contours of the Nusselt number at these positions are illustrated in Fig. 4.8 at $Re = 3.0\times10^4$. The heat transfer patterns are not different from each other globally, but, vary locally for each case. Focusing at the upstream region of the cylinder, it is found that the high heat transfer region is broader at lower distances between the vortex generators. The high heat transfer band was reduced by almost twice the width at the highest gap compared to the lowest gap. This high heat transfer region detached from the cylinder at an angle of about 80° and continued to decay in the downstream direction. This behavior was clearly visible at $S_z = 0.1$, then became week at $S_z = 0.25$ and for the larger gap it disappeared. This demonstrated that at lower gaps between the VG pair, the strength of the horseshoe vortex was increased as a result of strong coupling between the vortices produced by the VG pair and the cylinder and thus the heat transfer was enhanced. This coupling phenomenon can also be revealed from a relatively low heat transfer streak between the vortex generator and the cylinder at the higher gaps between the vortex generators. This low heat transfer streak continued in the downstream direction. Considering the downstream region of the cylinder, it was found that the wake region was not affected considerably by the lateral positions of the vortex generators. The size of the wake region was reduced by a small amount at the highest distance between the VG pair. The high heat transfer region, immediately after the wake region, was not changed significantly as far as the magnitude of the Nusselt numbers is concerned. For $S_z = 0.1$, the heat transfer enhancement was more due to the strong high heat transfer streaks appearing on both sides of the cylinder. However, the central high heat transfer region was not changed in magnitude and size with a change of the lateral spacing between the VGs despite a small decrease for $S_z = 0.5$.

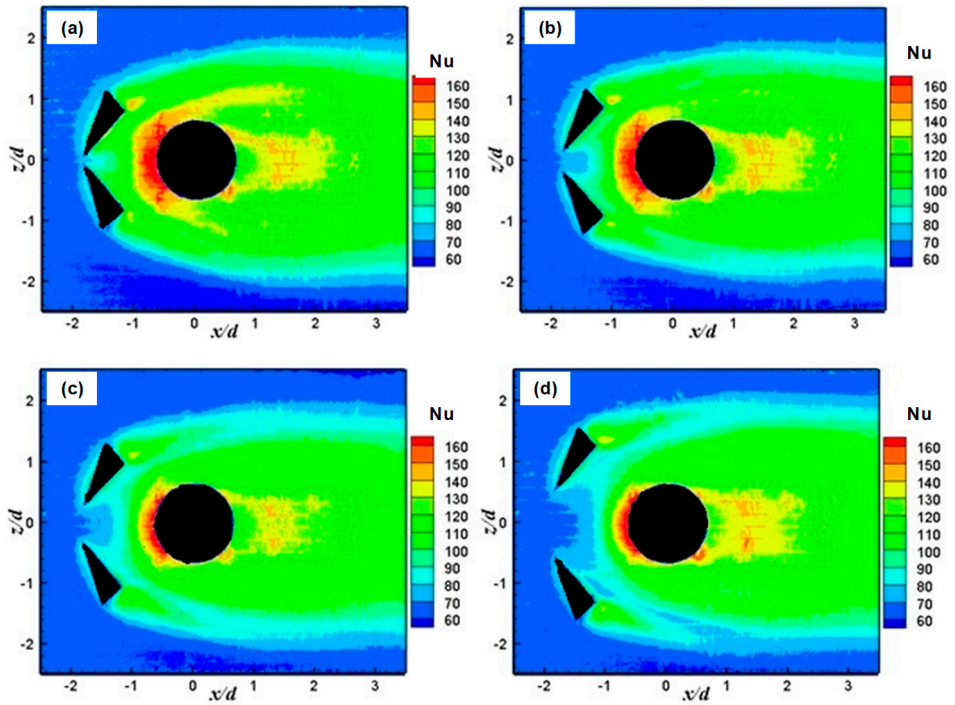

Figure 4.8: Nusselt number contours with VG pair at various spanwise positions, (a) S_z = 0.1 (b) S_z = 0.25 (c) S_z = 0.5 (d) S_z = 1.0.

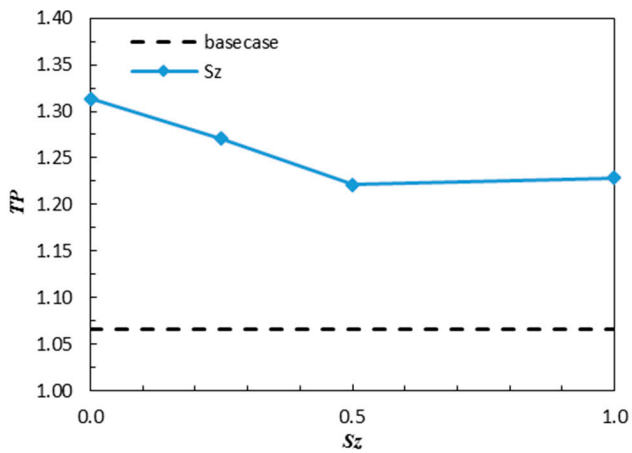

Figure 4.9: Thermal performance vs spanwise variation of the VG pair.

Thermal performance was also calculated and TP is shown in Fig. 4.9. Heat transfer was enhanced compared to the base case for all the lateral positions of the VGs. However, the enhancement was not the same for all the positions rather it depends on the lateral positions of the VGs. The highest value of the TP was achieved for the closest lateral distance between the vortex generators. Heat transfer enhancement in terms of TP decreased with the increase of S_z until $S_z = 0.5$ and from $S_z = 0.5$ to 1.0 it again increased by a small amount. Although the coupling was weak at $S_z = 1.0$, a small increase of TP can be attributed to the larger area of the heat transfer enhancement region due to the wide lateral spacing between the vortex generators.

4.2.4 Effect of Reynolds Number

The discussion above focused on a single Reynolds number (30,000). It is of paramount importance to investigate the effect of Reynolds number on the heat transfer enhancement with VGs. Therefore, from application perspective, Reynolds numbers from 20,000 to 50,000 were considered. In this study, the VG positions and angle was fixed based on the previous studies. The VGs were placed at a streamwise location of S_x=1.0 and spanwise location of S_z=0.25. Moreover, VGs were in CFI orientation with an attack angle of 45°. For brevity, only streamwise average Nusselt numbers are shown in Fig. 4.10. As depicted in Fig. 4.10, no clear difference was observed in the heat transfer pattern with the Reynolds number and obviously *Nu* increased with an increase of Reynolds number. However, at high Reynolds number (40,000 and 50,000), a small high heat transfer peak appeared at the location of the VGs.

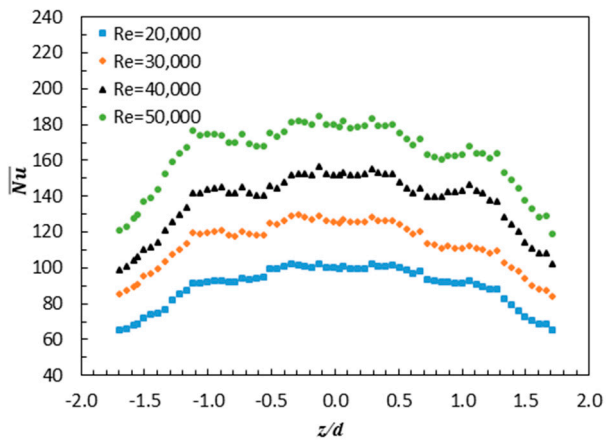

Figure 4.10: Streamwise averaged Nusselt numbers at different Reynolds numbers.

4.2.5 Effect of Height to Diameter Ratio

Figure 4.11 shows a comparison of the Nusselt number contours for a cylinder with height to diameter (*H/d*) ratio of 1 and 2 with and without VGs at a Reynolds number of 30,000. Further details on the results can be found in **Paper ii**. Focusing on the cases without the VG pair, no upstream change of the contours with the change of height to diameter ratio was noticed and thus, the height of the cylinder has no upstream effect.

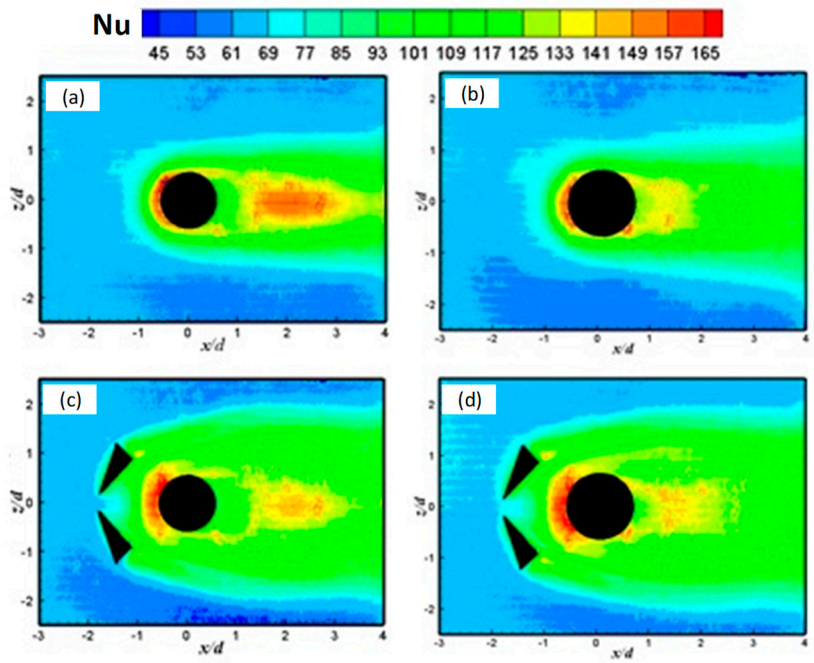

Figure 4.11: Nusselt number contours for cylinders with (a) *H/d* = 1 without VGs (b) *H/d* = 2 without VGs (c) *H/d* = 1 with VGs (d) *H/d* = 2 with VGs.

In the downstream region, the difference is enormous. This difference might be due to the additional vortices (Fig. 2.2) generated by the short cylinder with one end facing the flow. The wake region with low heat transfer was longer for the short cylinder than for the cylinder attached with both ends. Moreover, for the case with height to diameter ratio of 1, the high heat transfer region following the wake region increased in magnitude and was more elongated in the streamwise direction compared to its counterpart. This is because the tip and the arc vortices, might prolong the wake region and thus reattachment appears at the boundary further downstream. With the addition of the VG pair, the upstream high heat transfer band became thick with approximately the same order of magnitude for both cases again illustrating no change in the upstream region by the obstacle height. The phenomenon of thickening of the high heat transfer region has already been discussed in previous sections. In the downstream region, different behavior was observed for both cases. For *H/d*= 1, there is a

small spread in the wake region but the major difference is in the magnitude of the high heat transfer region. Its magnitude was decreased instead of increased compared to the corresponding base case but for the case with H/d= 2, the wake region and the high heat transfer region immediately after the wake region was not affected significantly either in position or magnitude. However, by close observation of Fig. 4.11*d*, there are two high heat transfer streaks that are visible on either side of the cylinder. These streaks look like a part of the high heat transfer band upstream of the obstacle and are detached from the cylinder surface and continued to decay in the downstream direction. It should be noted that, the overall heat transfer was increased in the downstream direction but this increase is more likely in the spanwise direction than in the streamwise direction.

Thermal performance was also calculated in order to evaluate the actual performance of the VG pair. The area averaged Nusselt number was calculated by Eq. (3.12) to obtain the TP using Eq. (3.11) and results are plotted in Fig. 4.12. As depicted in the figure, TP gradually decreases with the increase of Reynolds number for both cases. The Thermal Performance was higher for the cylinder with one end free in the flow than for the cylinder with both ends attached on the wall. This is because the short cylinder offered less pressure drop. Moreover, consistent behavior was observed for various Reynolds numbers.

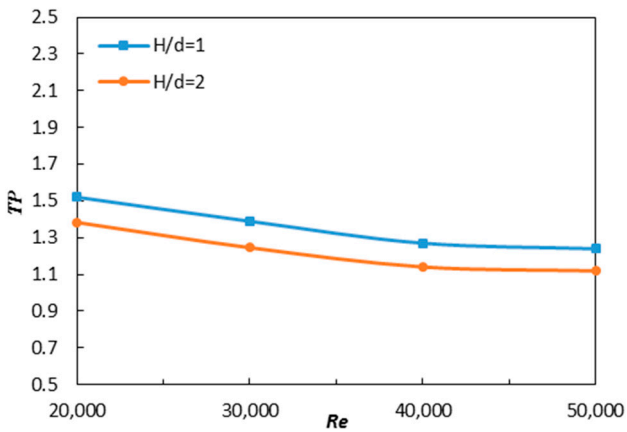

Figure 4.12: Thermal performance variation with Reynolds number.

4.3 Airfoil and VGs

The results presented in this section are obtained from **Papers iii** and **iv**. The endwall Nusselt number contours for large and small VGs are compared with base case in Fig. 4.13. The high heat transfer in the junction region for the base case is obvious due to the vortical motion in that region as described in chapter 2. However, in presence of VGs, the heat transfer in the junction was reduced significantly, particularly for the case with large VG. With small VG,

the magnitude of maximum value of *Nu* was not reduced but the bandwidth of the high heat transfer band was squeezed compared to the base case. On the other hand, both magnitude and width of the high heat transfer was suppressed significantly with large size of the VGs. It should be noted that the heat transfer was increased downstream of each VG due to the vortical motion associated with the VGs.

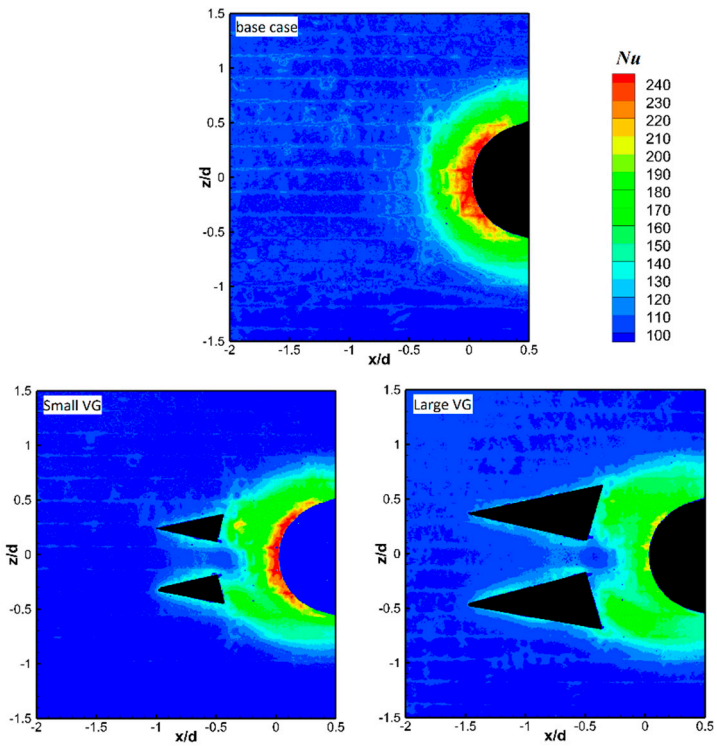

Figure 4.13: Experimental Nusselt number contours for small and large VGs compared with base case at $Re = 5.0\times10^4$.

A numerical study was conducted to get insight of the flow structures. The vorticity contours in the stagnation plane are shown in Fig. 4.14. Devenport and Simpson [105] presented similar type of vorticity patterns in their experiments. The largest magnitude of the negative vorticity indicates the position of the horseshoe vortex and its size and magnitude represent the size and strength of the HV, whereas the positive vorticity close to the leading edge of the airfoil illustrates the corner vortex. Fig. 4.14 clearly demonstrates that both size and strength of HV was suppressed by embedding the VGs in the boundary layer. Moreover, the large VG reduced the secondary flow more than the small VGs.

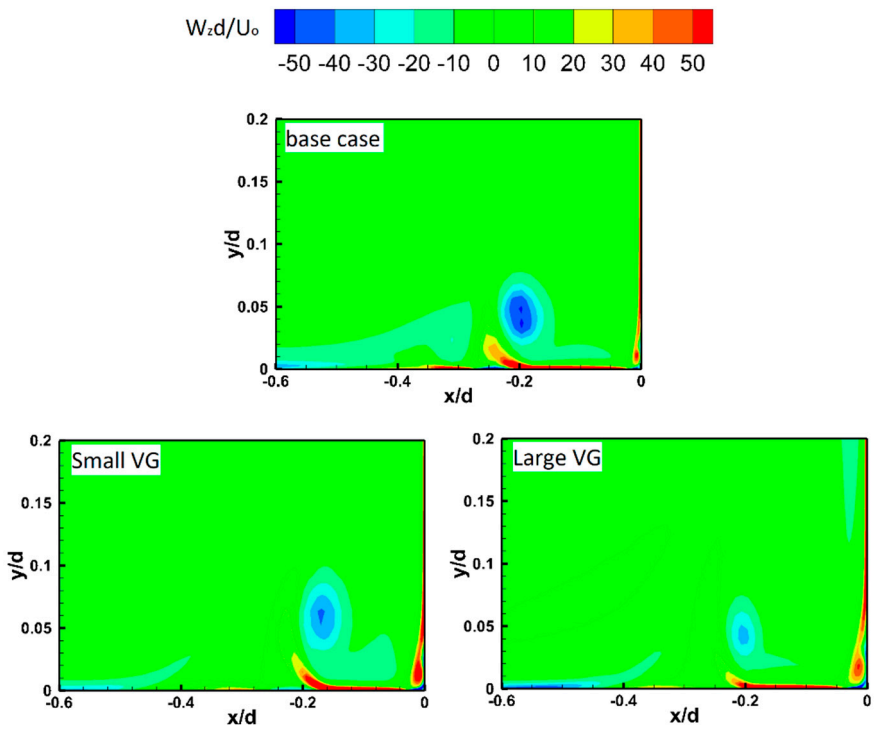

Figure 4.14: Vorticity contours for base case, large VG and small VG.

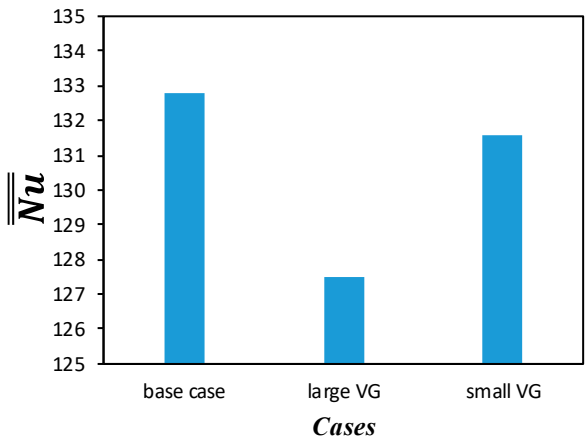

Figure 4.15: Area averaged Nusselt number.

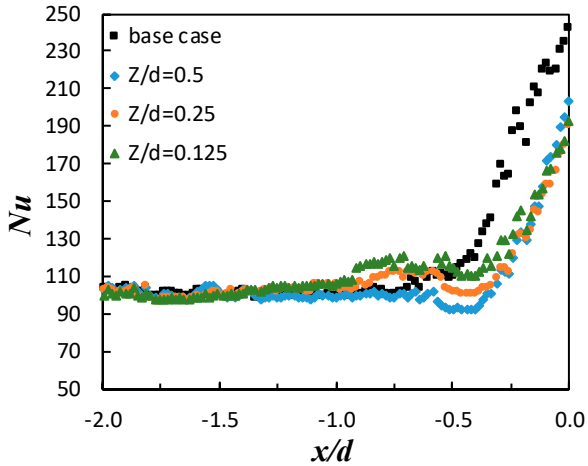

Figure 4.16: Nusselt number at the centerline for different cases.

Area averaged Nusselt numbers ($\overline{\overline{Nu}}$) calculated using Eq. (3.16) are presented in Fig. 4.15 which explains that the overall heat transfer in the junction region was reduced significantly. Moreover, it also shows that large VGs effectively degrade the heat transfer more than small VGs.

The Nusselt numbers in the upstream region of an airfoil at the symmetry line for large VGs placed at various spanwise positions are displayed in Fig. 4.16 together with the base case. In the far upstream region outside the junction region all the *Nu* curves overlap showing no effect of VGs in that region but illustrating the repeatability of the experiments. However, in the junction region, VGs played an extraordinary role by reducing the heat transfer in that region. The peak value of the Nusselt number was found lower with VGs than without VGs (base case) with a maximum reduction upto 23% for VGs placed at a spanwise gap of *Z/d*=0.25, which suggests an optimal gap. Moreover, a dip of the center line *Nu* was also observed at the streamwise location of the VG trailing ends (*x/d* = -0.5) but here VGs spanned at a large gap (*Z/d*=0.5) offered more reduction in *Nu*.

Flow features obtained numerically are presented in Fig. 4.17 in the form of streamlines at the stagnation plane. The flow structures highlight the modification and suppression of heat transfer in the junction region. First of all, referring to the streamlines for the case without VGs, like the past literature studies of Praisner and Smith [7], four types of vortical structures are obtained as horseshoe vortex, corner vortex, secondary vortex and tertiary vortex. In the presence of the VGs, these vortical patterns were modified as the boundary layer approaching the airfoil was disturbed by the VGs. The streamline deterioration greatly depends on the spanwise gap between the VGs. The streamlines are lifted off from the boundary layer due to the up wash phenomenon of the vortices associated with the VGs because the VGs were installed in counter flow outward (CFO) orientation. This is the reason why vortices especially HV showed elongated shape in the vertical direction. The lifting of streamlines actually

degraded the heat transfer on the endwall. At a moderate gap between VGs, the SV disappeared while TV lost its size, a manifestation of heat transfer reduction in that case.

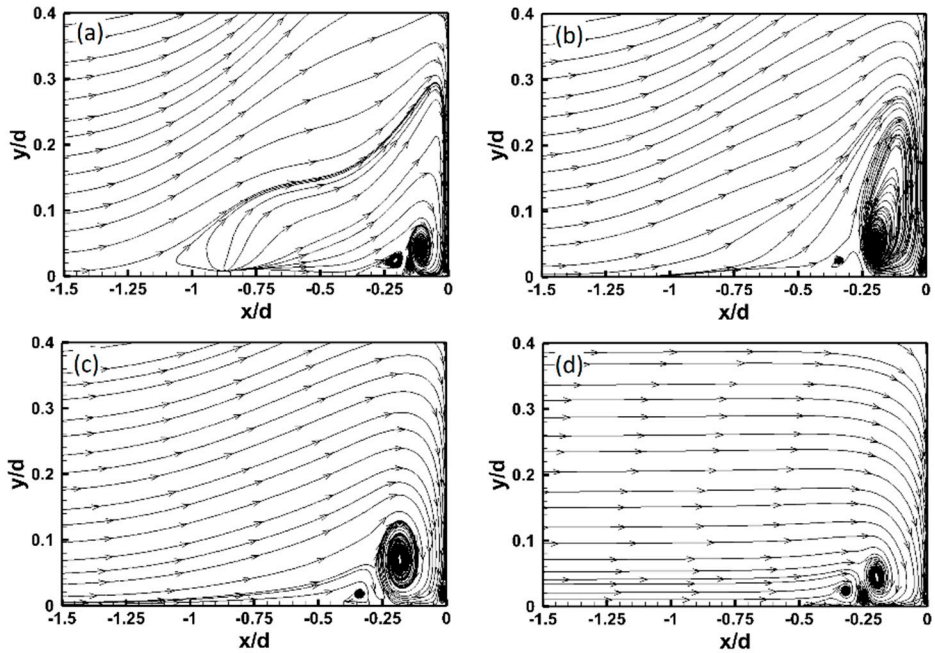

Figure 4.17: Streamlines at stagnation plane for the VGs at various positions and base case.

4.4 Airfoil and Cavity

The experimental endwall Nusselt number contours around the airfoil are shown in Fig. 4.18 for a Reynolds number of 87,600. The heat transfer patters for other Reynolds numbers are similar and therefore are not presented here (for details refer to **Paper v**). The region mentioned as blocked area in Fig. 4.18 is without any heat transfer data since this region was invisible by the camera. For the case without cavity (case 0) the heat transfer in the junction region like the previous study showed high heat transfer due to the associated vortices. For cases with cavity, the high heat transfer is reduced significantly. The reduction of heat transfer is greatly dependent on the distance between the cavity and the airfoil. The reduction of heat transfer in the junction region can be attributed to the change in flow structure as a result of the cavity. This is obvious as the cavity disrupts the boundary layer and after the cavity the boundary layer starts to redevelop and therefore as the distance between the cavity and airfoil increases the boundary layer approaches to the smooth channel case. A small increase in Nusselt number was observed at the immediate exit of the cavity and this is clearly visible for Case 1.

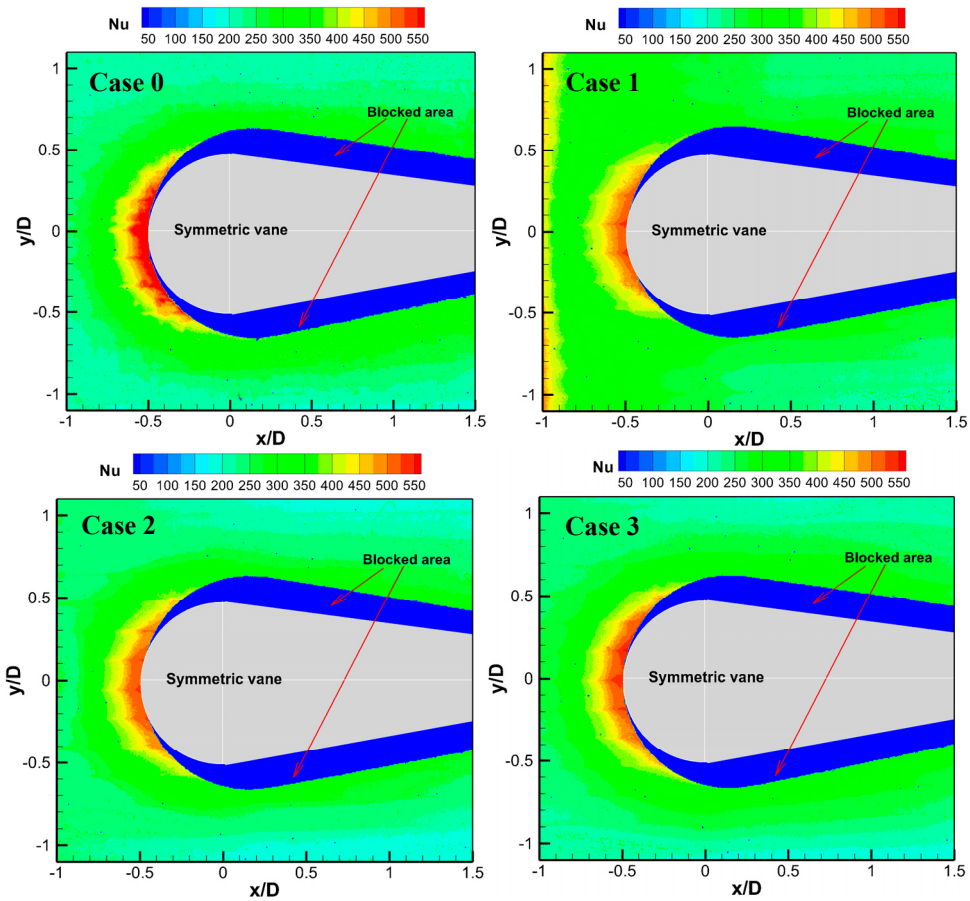

Figure 4.18: Nusselt number contours for different cases (Reynolds number = 87600).

To get insight of the flow characterization, streamlines at the stagnation plane and pressure coefficients (C_p) on the endwall are displayed in Fig. 4.19. The pressure coefficients on the endwall are similar to the heat transfer distribution on the endwall. The high magnitudes of C_p in the junction region and downstream of the cavity represent the strong flow impingement on the endwall and hence high heat transfer. Moreover, the strength of the pressure coefficient varies differently for the three cases with cavity representing different magnitudes of heat transfer. The streamlines in the junction region show the flow impingement as a result of vortices generated in that region. Stronger vortices give stronger heat transfer as the vortices in the junction for the smooth channel case were stronger than the other cases. For cases with the cavity, the strength of vortices varied from case to case. A strong recirculating flow occurred inside the cavity and its strength varied depending on the distance between the cavity

and the vane. In this case, the strong vortical flow within the cavity was observed for case 1 which has the smallest gap.

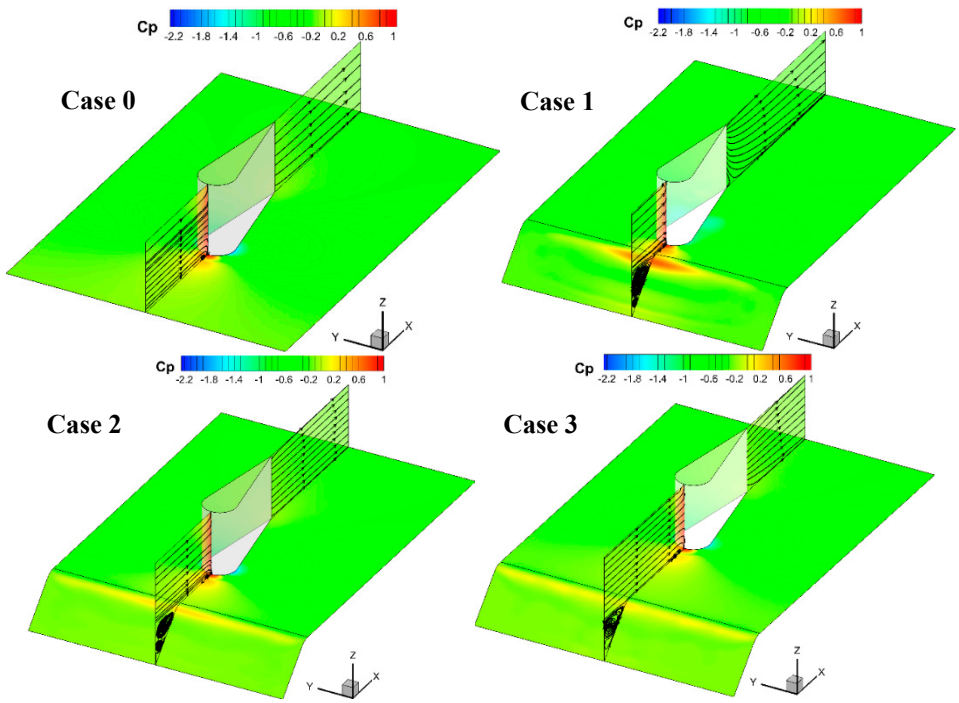

Figure 4.19: Stagnation plane streamlines with endwall pressure coefficients.

4.5 Pin Fins with VGs

The contours of Nusselt number on the endwall of the test section wedge duct with VGs mounted at different angles and the base case (without VGs) are shown in Fig. 4.20 for a Reynolds number of 30,000. Detailed results are available in **Paper vi**. The *Nu* in the upstream of each pin fin for the base case showed enhanced heat transfer due to the HV and the enhancement was further promoted with VGs. On the other hand, downstream of the pins, a wake region depicting low heat transfer region was observed. Enhanced heat transfer in the streamwise direction appeared for all cases and this is due to the vortical flow interaction between the neighboring pin fins in addition to increased velocity effect due to the wedge shaped of the channel. Interestingly, the influence of VGs is transmitted through the whole downstream region although VGs were employed only upstream of the first row of pin fins. Most importantly, the *Nu* was increased significantly between the rows of pin fins in the streamwise direction as a result of VG vortices interaction which otherwise was poor without

VGs. This is particularly dependent on the VGs angle of attack and VGs at high angle (45°) showed higher effectiveness.

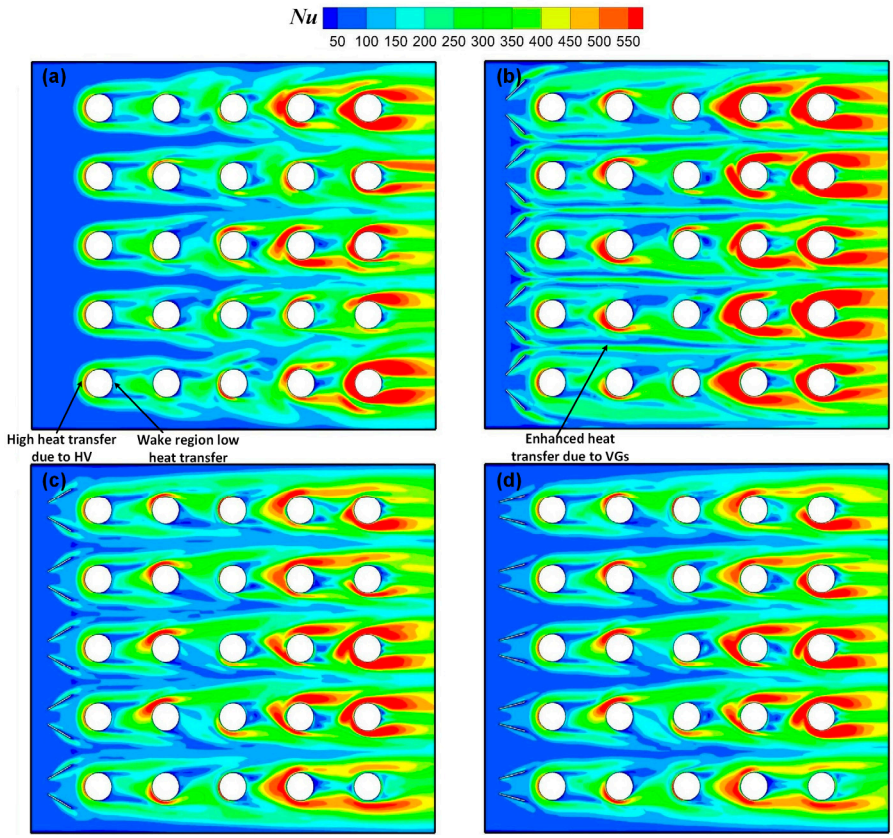

Figure 4.20: Endwall Nusselt number contours at *Re* = 30,000 for (a) base case (b) VGs at 45° (c) VGs at 30° (d) VGs at 15°.

The phenomenon of heat transfer enhancement with VGs can be clearly understood by 3D streamlines shown in Fig. 4.21 in which the streamline color represents the airflow temperature. The HV causing high heat transfer wrapped the pin fins on both sides. The HV strength is magnified as one moves in the streamwise direction due to the vortices interaction with the subsequent pin fins. Moreover, the colors of the streamlines also changed in that direction again illustrating the phenomenon of heat transfer enhancement. In the presence of the VGs, the strength of the HV is enlarged as a result of coupling of vortices generated by the VGs. The high heat transfer for the case with VGs at 45° can be understood by the more complex and distorted streamlines.

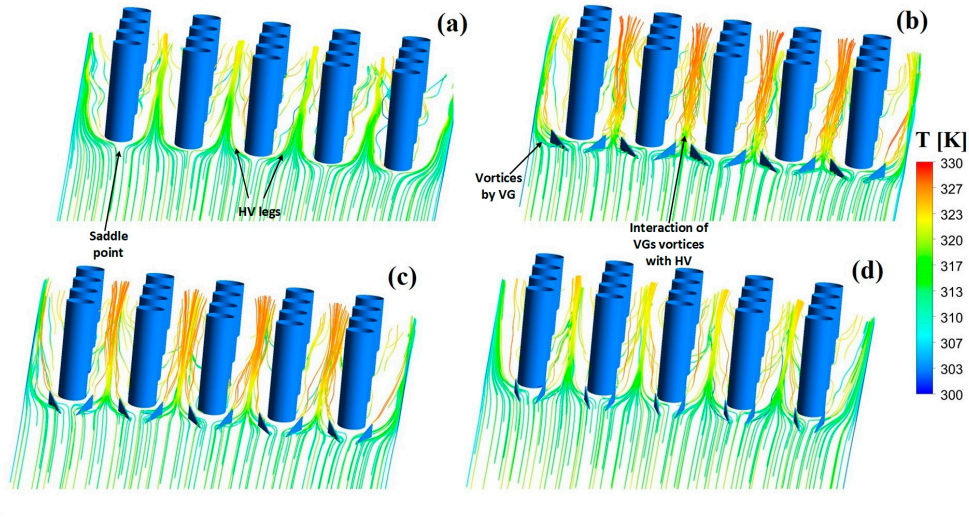

Figure 4.21: Three dimensional streamlines without VGs and with VGs at various angles (a) base case (b) VGs at 45º (c) VGs at 30º (d) VGs at 15º.

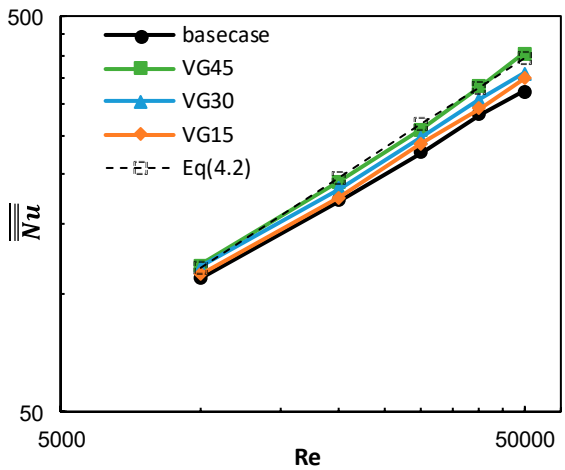

Figure 4.22: Area averaged Nusselt numbers on endwall for different cases.

To estimate the overall enhancement of heat transfer with VGs, area averaged Nusselt numbers ($\overline{\overline{Nu}}$) are compared with the base case in Fig. 4.22 for a range of Reynolds numbers.

As depicted from the Fig. 4.22, the overall heat transfer was improved with the installation of VGs and VGs placed at 45° presented superior performance. Furthermore, the heat transfer performance was augmented for all Reynolds numbers but higher Reynolds number promoted the heat transfer. This might be due to the thin boundary layer at high Reynolds number which might be completely disturbed by the VGs since VGs with small height were used. Many correlations were developed in the past related to pin fin heat transfer and proposed by Hwang and Lui [98], Metzger [106] and Chyu et al. [107]. Following the former procedure, correlations presented in Eq. (4.1) and Eq. (4.2) were developed based on the present investigation for the base case and a case with VGs at 45°, respectively.

$$\overline{\overline{Nu}} = 0.203Re^{0.682} \tag{4.1}$$

$$\overline{\overline{Nu}} = 0.103Re^{0.762} \tag{4.2}$$

The correlations suggested by Hwang and Lui [98] ($\overline{\overline{Nu}} = 0.168Re^{0.692}$) and Chyu et al. [107] ($\overline{\overline{Nu}} = 0.155Re^{0.658}$) are consistent with the present base case thus reinforcing validation of the present study. In the latter case, the small value in the exponent of *Re* might be due to different ranges of Reynolds number. The high dependency of heat transfer on Reynolds number in presence of the VGs was also visibly and reflected in the exponent of *Re* in Eq. (4.2) which is higher than for the base case.

After getting enhanced heat transfer enhancement with VGs, investigation was further carried out to study the streamwise distance between pin fins and VGs by keeping the VGs at 45° because that benefitted most. For brevity only thermal performance defined in Eq. (3.18) is shown in Fig. 4.23 along with thermal performance with VGs placed at various angles. It is obvious that mounting VGs imposes additional pressure loss, but the thermal performance is higher than the base case illustrating the true advantage of VGs. Thermal performance is more sensitive to VG angle than the streamwise gap between VGs and pin fins. Similar to the base case, TP decreased with Reynolds number for all cases. However, the magnitude of the difference of TP between the case with and without VGs increases with Reynolds number predominantly with VGs at 45° thus providing more favorable heat transfer enhancement. Similar, a moderate gap (x/d=1) between the VGs and pin fins was better than other gaps.

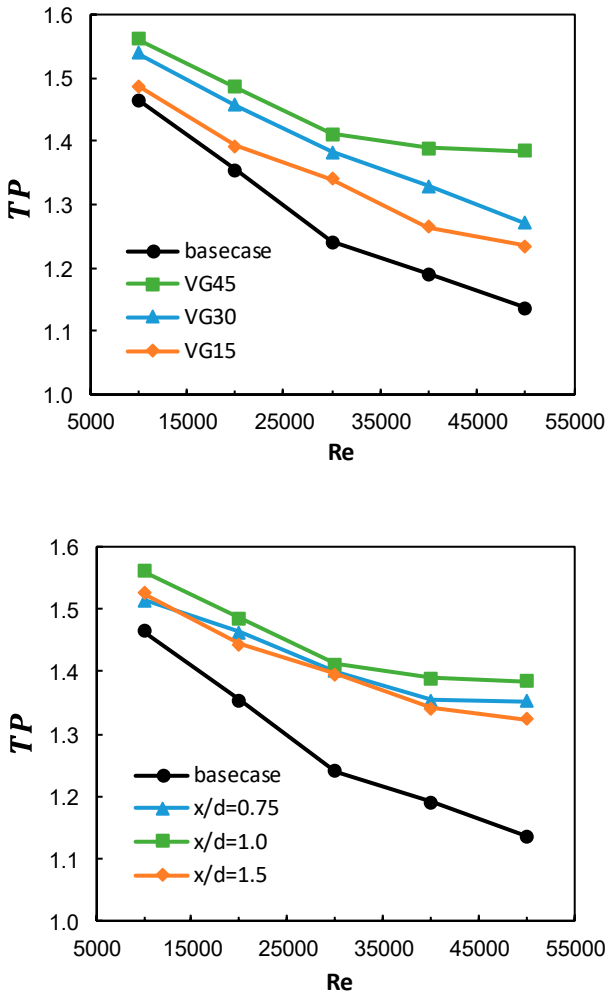

Figure 4.23: Endwall thermal performance for different cases.

4.6 Axisymmetric Endwall Contouring

Some of the results from **Paper vii** are presented in this section. The contours of film cooling effectiveness obtained from the numerical study are displayed in Fig. 4.24 for all the investigated cases. Figure 4.24 revealed that the effect of slot cooling is asymmetric around the stagnation plane which is evident from the non-uniform pressure distribution around the

NGV. Most of the coolant from the slot made its way to the suction side (SS) due to the high pressure on the pressure side (PS) of the NGV and thus enhanced the effectiveness on the suction side. By applying contouring on the endwall (C_1, C_2), the slot coolant achieved favorable circumstances to expand the region where film cooling is active. For C_2, the coolant from the slot cooled the endwall effectively and better than the case C_1 and of course the flat endwall (C_o). More importantly, a vast region of the endwall near the pressure side remained uncooled for case C_o (flat endwall) but it gained significant film cooling effectiveness when contouring was used on the endwall especially for a large contouring angle (α=25°) and in that case the coolant covered the whole region on the pressure side to the NGV wall although it weakened very close to it. Moreover, the effectiveness is least effective in the symmetry line for flat endwall due to the strong adverse pressure gradient. However, it was improved by the contoured endwall cases and is proportional to the contouring angle.

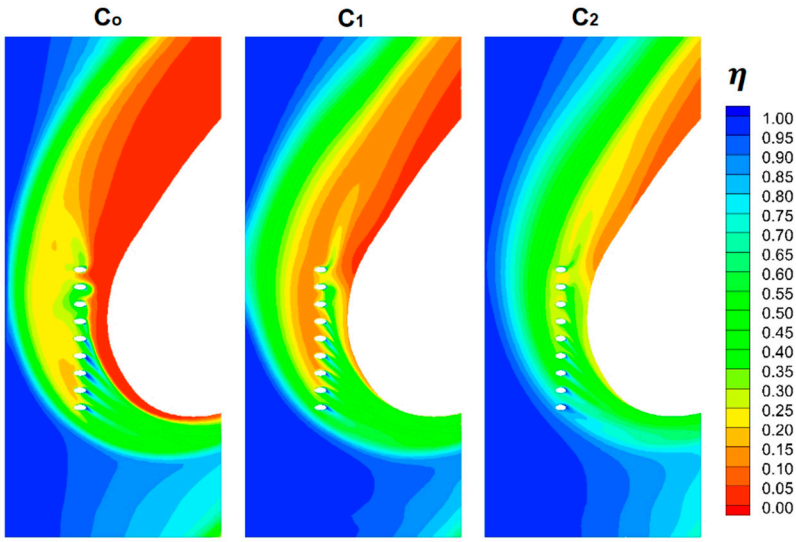

Figure 4.24: Film cooling effectiveness with and without endwall contouring.

The film cooling effectiveness from discrete holes was largely defected by the endwall contouring. As the film cooling holes on the endwall are close to the leading edge junction of the NGV, where strong vortical flow exists, a region appeared near the junction of NGV with no film cooling effectiveness for the flat endwall. This uncooled region slightly narrowed down on the suction side. However, it extended and coupled the large uncooled part both for the slot and discrete film cooling on the pressure side. Particularly, the effectiveness from the film cooling holes near the stagnation line did not show any significant effectiveness because the coolant jet was lifted due to the horseshoe vortex generated in that region. On the other

hand, the uncooled region near the leading edge of the NGV is associated with very high heat transfer and therefore it must be sufficiently cooled to avoid worse situations from a practical point of view. Much improved conditions prevailed for the C_1 and C_2 cases. The coolant covered the uncooled junction region effectively with C_2 being more productive for film cooling effectiveness.

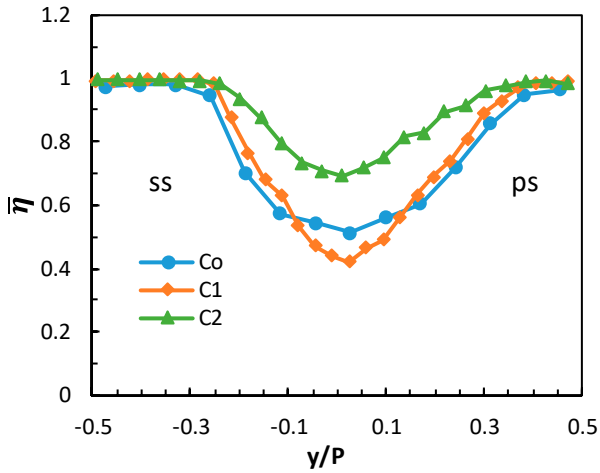

Figure 4.25: Streamwise averaged film cooling effectiveness.

To reveal the behavior of the film cooling effectiveness in the spanwise direction, the streamwise averaged film cooling effectiveness from the slot axial position to the junction of the leading edge was calculated and shown in Fig. 4.25. The shape of $\bar{\eta}$ is like an inverted bell with minimum effectiveness around $y/P \sim 0$, similar for all cases. The film cooling effectiveness was significantly improved with contouring especially at a contoured angle of 25°. The effectiveness lowest value was improved up to 40% for C_2 case which is a significant step forward to enhance the effectiveness in the junction region. The Film cooling effectiveness extreme value was consistent for all cases but occupied a larger region on the suction side than on the pressure side.

Similarly, the spanwise averaged effectiveness is presented in Fig. 4.26. At the immediate exit of the slot x/C =-0.1 film cooling effectiveness was quite high with a large magnitude for C_2 compared to C_o and C_1 cases. It dropped steadily up to the upstream position of the discrete film cooling holes followed by a steep rise at the position of film cooling holes. It again followed a similar trend as the slot cooling and dropped to its lowest value at the stagnation point (x/C=0). Importantly, at the stagnation, the film cooling effectiveness is significantly high with contouring compared to the flat endwall and the case C_2 offered better enhancement. Furthermore, after the stagnation point, it again raised but slowly and achieved another peak value. After the peak value, $\bar{\eta}$ continued to decline asymptomatically in the downstream

direction. It is important to mention that even in the region $x/C > 0$ the film cooling effectiveness appeared much higher than for the flat endwall case with C_2 as the leading case.

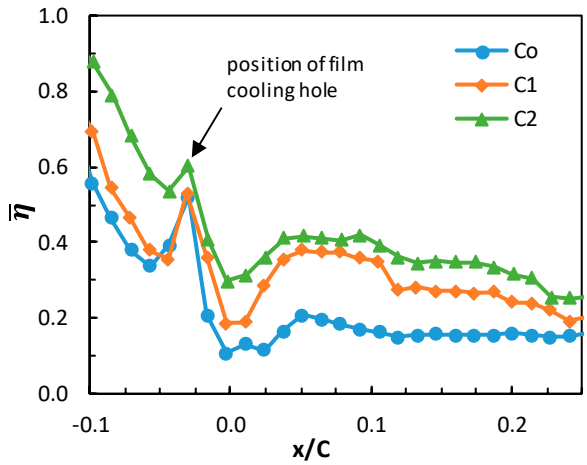

Figure 4.26: Spanwise averaged film cooling effectiveness on endwall.

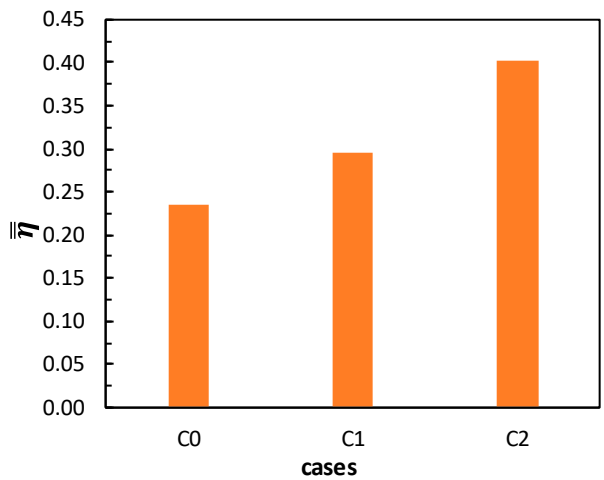

Figure 4.27: Area-averaged film cooling effectiveness for three cases.

In the preceding discussion, the streamwise and spanwise averaged film cooling effectiveness was discussed. It is also important to compare the area averaged effectiveness ($\bar{\bar{\eta}}$) with and without contoured endwall and this is shown in Fig. 4.27. Figure 4.27 clearly demonstrates

how the contouring improves the film cooling. Moreover, it presents that the effectiveness increases with the contour angle (α) and for a contoure angle of $\alpha = 25^{o}$ (C_2) about 70 % enhancement was found compared to the flat contoured endwall.

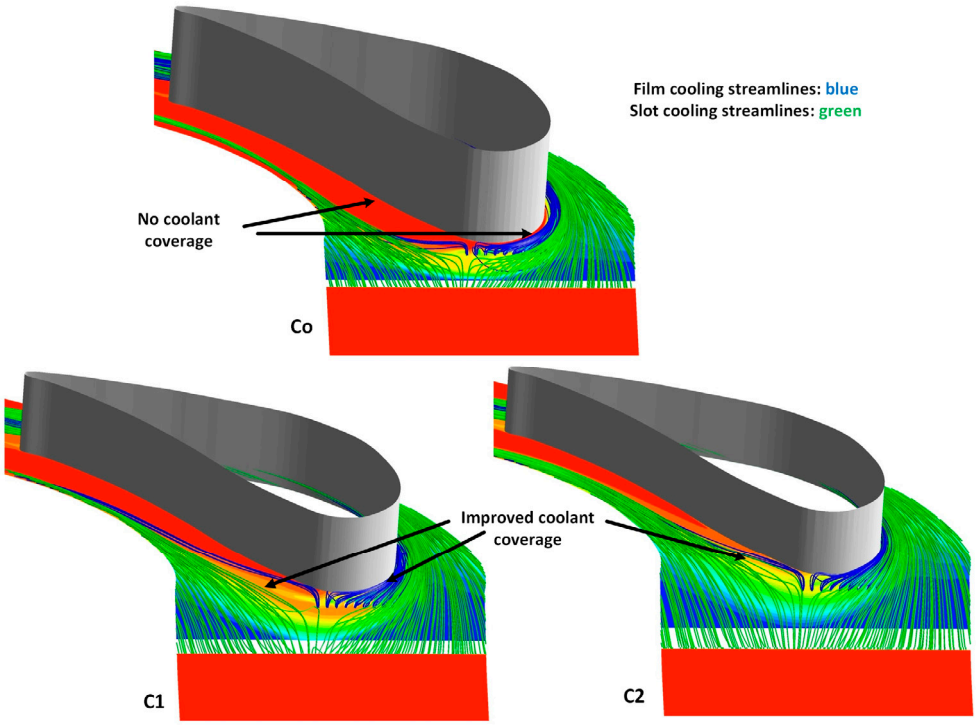

Figure 4.28: Streamlines from slot and film cooling holes.

Streamlines in Fig. 4.28 illustrate the understanding of the flow physics behind the improvements in the film cooling with the contoured endwall in the form of 3D streamlines with contours of film cooling effectiveness on the endwall. The blue and green streamlines represent the coolant from the discrete film holes and slot, respectively. The streamlines emanating from the slot are not uniform instead most of the streamlines are diverted towards the suction side being less efficient for the flow and hence demonstrated high film cooling effectiveness on the suction side. Similarly, no streamlines were approaching towards the region on pressure side of the NGV where there was no coolant coverage instead streamlines made their way far away from the pressure side. Moreover, few streamlines on the symmetry line was observed again depicting low effectiveness along the streamwise axis. In the case of endwall contouring, the suction side did not change too much, however, streamlines pattern on the pressure side changed significantly. The streamlines travelled a longer distance downstream before sweeping on the either side of the NGV and thus covered a larger region for slot cooling. Moreover, more interestingly, a large region of the endwall on the pressure

side was without any streamlines for the flat case but it reduced into a small region when contouring was employed.

The streamlines belonging to film cooling from the discrete holes and streamlines from all the holes except the one on the pressure side swept on the suction side. It seemed that the streamlines followed the horse shoe vortex as the streamlines rolled up in the form of vortices. Due to the rolling up of the streamlines, an uncooled region close to the junction of the NGV appeared. It is clearly visible in Fig. 4.28 for Case C_o. The rolling up of the streamlines was weakened due to the weak HV as a result of contouring. Therefore, streamlines covered the uncooled region in the junction region (Cases C_1 and C_2), which is extremely hot due to high heat transfer.

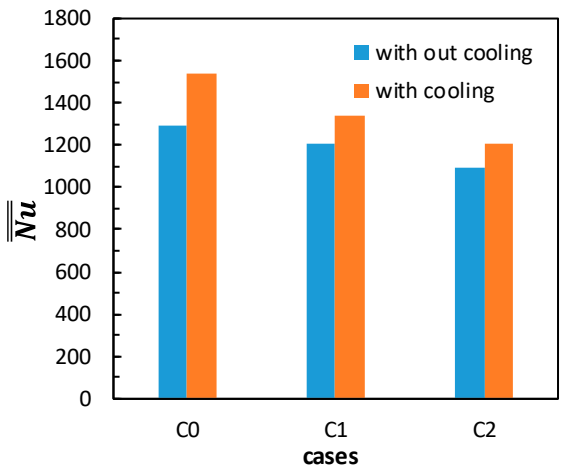

Figure 4.29: Area averaged Nusselt number with and without film cooling flow.

Together with the film cooling effectiveness study, a heat transfer study was conducted both with and without film cooling to find out the effect of heat transfer with film cooling. For conciseness, only area averaged Nusselt numbers are presented in Fig. 4.29 although a detailed study has been made. Figure 4.29 demonstrates many features regarding heat transfer. The endwall heat transfer is reduced by the contoured endwall and the level of reduction is dependent on the contour angle and increases with the increase of contour angle. Additionally, the Nusselt number suppression is also influenced by the state of film cooling as it is reduced 21% and 15.6 % for case C_2 with film cooling and without film cooling, respectively. Moreover, the heat transfer increased with the implementation of film cooling compared to without film cooling both for the flat and contoured endwall. But the rise in heat transfer with film cooling was more for the flat endwall than for the contoured endwall. As depicted in Fig. 4.29, the area averaged Nusselt number increased 18 % for C_o with the inclusion of film cooling whereas, it was increased only 11% for C_1 which is 38.9 % less compared to the former case.

CHAPTER 5

Conclusions

The study presented in this thesis was aimed to increase the heat transfer performance in gas turbines with an objective to boost the gas turbine thermal efficiency as a result of increased gas turbine inlet temperature. The study is based on various aspects of gas turbines, starting from fundamental ones to more applied ones.

Initially, as a fundamental study, a pair of longitudinal winglet vortex generators (VGs) was installed upstream of a cylindrical obstacle. Various parameters of VGs like the streamwise and spanwise position of the VGs relative to the obstacle, orientation and angle of attack of the VGs were investigated experimentally using liquid crystal thermography. The following major outcomes arose:

- Counter flow inward orientation (CFI) of the VG pair upstream of an obstacle can be used for endwall heat transfer augmentation whereas, counter flow outward (CFO) is appropriate for reduction of endwall heat transfer.
- The position of the VG pair relative to the obstacle changed the local heat transfer pattern on the endwall by up to 25% heat transfer augmentation with only a pressure drop increase of 4.8%.
- VGs placed at a yaw angle of 45º showed more efficient behavior regarding endwall heat transfer enhancement than smaller yaw angles.
- Thermal performance in presence of vortex generators is higher for the cylinder having one end in the flow than for the cylinder with both ends fixed to the walls.

VGs were employed with an airfoil representing a gas turbine nozzle guide vane. A pair of longitudinal winglet vortex generators was employed upstream of a symmetric airfoil in counter flow outward (CFO) orientation at an angle of 15°. The streamwise gap between the VGs and vane was fixed but various spanwise distances between the VGs were investigated experimentally whereas, simulations were also performed to get insight of the flow structure.

Moreover, by considering the more practical situation, outlet guide vanes (OGVs) are used to straighten the swirled flow that exit from the low pressure turbine in aero engine. In modern advanced aero engines, a cavity is formed as assembling of the engine is performed. Therefore, a triangular cavity upstream of a symmetric vane (representing OGV) was investigated. Various gaps between the cavity and vane was investigated both experimentally and numerically.

The main conclusions drawn from these investigations are outlined as:

- The size of the VGs played a significant role on the degradation of heat transfer in the junction region with large VGs being more efficient for degradation.
- The magnitude and bandwidth of heat transfer upstream of a vane was reduced when VGs were at a moderate distance apart.
- The numerically study predicted that the strength of HV was reduced with VGs which is supposed to be responsible for lowering the heat transfer.
- Like the VGs, a cavity upstream of an OGV reduced the heat transfer in the junction region compared to the without cavity case by altering the flow approaching the airfoil. However, in this case, the cavity located close to the vane showed more heat transfer reduction.

For real gas turbine applications, focus was on the trailing part of the gas turbine internal cooling where typically pin fins are employed. Pairs of vortex generators upstream of the first row of five rows pin fin arrays were investigated numerically using ANSYS Fluent. Using the knowledge gained from the fundamental study of this thesis, VGs were mounted in counter flow inward (CFI) orientation and a fixed spanwise distance between the VGs were maintained. Different streamwise positions and angle of attacks were investigated and concluding remarks from this investigation are:

- Thermal performance improved with the addition of VGs compared to without VGs. Like the base case, thermal performance decreased with Reynolds number but the level of degradation was not as much as for the base case.
- Investigation of the angle of attack revealed that VGs at 45° angle of attack are more appropriate for thermal performance enhancement.
- The thermal performance was not as much dependent on the streamwise positions of VGs as the angle of attack, however, a moderate position of VGs showed better performance.

In the last part of the thesis the assembly of the first stage nozzle guide vane (NGV) with the combustor using axisymmetric endwall contouring was numerically (ANSYS Fluent) investigated. The effect of endwall contouring on the film cooling performance from the slot and discrete film cooling holes placed in the leading edge junction region were studied. Two angles of endwall contouring were comparatively studied along with the base case (without contouring). Conclusions obtained are:

- The uncooled region in the vicinity of the leading edge of the NGV gained significant coolant coverage with the contouring on the endwall. Similarly, a large part of the endwall region on the pressure side remained uncooled for the base case but film cooling effectiveness was also improved in this region with contouring.
- The heat transfer in the junction region was reduced by the application of endwall contouring.
- The strength of the HV and secondary flow generated upstream of NGV were suppressed by the contoured endwall compared to the flat endwall.

CHAPTER 6

Future Work

The research work presented in this thesis has a large scope in engineering applications especially in gas turbines and therefore can be extended in future perspectives in a variety of ways both experimentally and numerically. Few suggested studies are listed below:

- In present study, only one shape of the VG was investigated, however various other shapes of VG exist in literature, so study of other VG shapes might be potentially useful in future investigations.
- Although RANS based numerical simulations were performed here but to get more insight into the dynamic behavior of the vortices associated with obstacle/pin fins and VGs, transient simulations based on Detached Eddy Simulation (DES) or Large Eddy Simulation (LES) are proposed.
- Extending the experiments, particle image velocimetry (PIV) is recommended to visualize the flow physics for the investigations in this thesis and as well as to provide data for validation of numerical studies.
- In the pin fin study, only one size and shape of the VGs were investigated with an inline arrangement of pin fin arrays. A similar study could be extended to optimize the shape and size of VGs for thermal performance enhancement for different configurations and shapes of pin fins.
- An experimental study in a linear turbine cascade with a VG pair upstream of a vane is highly useful for investigations of heat transfer reduction in the junction region and some other characteristics. Moreover, the heat transfer behavior on the surface of the VG is highly important, as in real engine conditions VGs placed in the upstream of a vane might fail due to exposure to high temperature.

- For axisymmetric endwall contouring, high angle of endwall contouring on one or both walls as well as nonlinear axisymmetric endwall contouring could be of interest. Also, the location of NGV with reference to contouring is another parameter that needs to be investigated.

References

[1] Mamaev, B.I., Internal Communication, Siemens LLC Energy Oil and Gas Department, 2011.

[2] Bathie, W.W., Fundamentals of Gas Turbines, 2nd ed. 1996, John Wiley and Sons, New York.

[3] Pratt and Whitney, 2019, Accessed 4 April 2019, https://www.pw.utc.com/products-and-services/products/commercial-engines/GP7200-Engine/

[4] Yuri, M., Masada J., Tsukagoshi, K., Ito, E., Hada, S., Development of 1600 C-class high-efficiency gas turbine for power generation applying J-Type technology, *Mitsubishi Heavy Industries Technical Review*, 2013, **50**(3), pp. 1-10.

[5] Eckerle, W.A., Langston, L., Horseshoe vortex formation around a cylinder, *ASME Journal of Turbomachinery*, 1987, **109**, pp. 278-285.

[6] Sharma, O.P., Butler, T.L., Predictions of endwall losses and secondary flows in axial flow turbine cascades, *ASME Journal of Turbomachinery*, 1987, **109**, pp. 229-236.

[7] Praisner, T., Smith, C., The dynamics of the horseshoe vortex and associated endwall heat transfer-part II: time-mean results, ASME *Journal of Turbomachinery,* 2006, **128**(4), pp. 755-762.

[8] Fleming, J.L., Simpson, R., Cowling, J., Devenport, W., An experimental study of a turbulent wing-body junction and wake flow, *Experiments in Fluids*, 1993, **14**(5), pp. 366-378.

[9] Ozturk, N.A., Akkoca ,A., Sahin, B., Flow details of a circular cylinder mounted on a flat plate, *Journal of Hydraulic Research*, 2008, **46**(3), pp. 344-355.

[10] Kang, M., Thole, K.A., Flowfield measurements in the endwall region of a stator vane, *ASME Journal of Turbomachery*, 2000, **122**(3), pp. 458-466.

[11] Sahin, B., Ozturk, N.A., Akilli, H., Horseshoe vortex system in the vicinity of the vertical cylinder mounted on a flat plate, *Flow Measurement and Instrumentation*. 2007, **18**(2), pp. 57-68.

[12] Pattenden, R., Turnock, S., Zhang, X., Measurements of the flow over a low-aspect-ratio cylinder mounted on a ground plane, *Experiments in Fluids*, 2005, **39**(1), pp.10-21.
[13] Kang, M.B., Kohli. A., Thole, K.A., Heat transfer and flowfield measurements in the leading edge region of a stator vane endwall, ASME *Journal of Turbomachinery*, 1999, **121**(3), pp. 558-568.
[14] Satta, F., Tanda, G., Measurement of local heat transfer coefficient on the endwall of a turbine blade cascade by liquid crystal thermography, *Experimental Thermal and Fluid Science*, 2014, **58**, pp. 209-215.
[15] García-Villalba, M., Palau-Salvador, G., Rodi, W., Forced convection heat transfer from a finite-height cylinder, *Flow, Turbulence and Combustion*, 2014, **93**(1), pp. 171-187.
[16] Nakamura, H., Igarashi, T., Tsutsui, T., Local heat transfer around a wall-mounted cube in the turbulent boundary layer, *International Journal of Heat and Mass Transfer*, 2001, **44**(18), pp. 3385-3395.
[17] Goldstein, R., Chyu, M., Hain, R., Measurement of local mass transfer on a surface in the region of the base of a protruding cylinder with a computer-controlled data acquisition system, *International Journal of Heat and Mass Transfer*, 1985, **28**(5), pp. 977-985.
[18] Wang, H., Zhou, Y., Chan, C., Zhou, T., Momentum and heat transport in a finite-length cylinder wake, *Experiments in Fluids*, 2009, **46**(6), pp. 1173-1185.
[19] Chen, S., Sanitjai, S., Ghosh, K., Goldstein, R., Three-dimensional vortex flow near the endwall of a short cylinder in crossflow: uniform-diameter circular cylinder, *Applied Thermal Engineering*, 2012, **49**, pp. 73-78.
[20] Goldstein, R., Yoo, S., Chung, M., Convective mass transfer from a square cylinder and its base plate, *International Journal of Heat and Mass Transfer*, 1990, **33**(1), pp. 9-18.
[21] Sparrow, E., Stahl, T., Traub, P., Heat transfer adjacent to the attached end of a cylinder in crossflow, *International Journal of Heat and Mass Transfer*, 1984, **27**(2), pp. 233-242.
[22] Hinckel, J.N., Nagamatsu, H.T., Heat transfer in the stagnation region of the junction of a circular cylinder perpendicular to a flat plate, *International Journal of Heat and Mass Transfer*, 1986, **29**(7), pp. 999-1005.
[23] Yoo, S., Goldstein, R., Chung, M., Effects of angle of attack on mass transfer from a square cylinder and its base plate, *International Journal of Heat and Mass Transfer*, 1993, **36**(2), pp. 371-381.
[24] Chyu, M., Natarajan, V., Heat transfer on the base surface of threedimensional protruding elements, *International Journal of Heat and Mass Transfer*, 1996, **39**(14), pp. 2925-2935.
[25] Yan, W., Hsieh, R., Soong, C., Experimental study of surface-mounted obstacle effects on heat transfer enhancement by using transient liquid crystal thermograph, *Journal of Heat Transfer*, 2002, **124**(4), pp. 762-769.
[26] Wang, L., Salewski, M., Sundén, B., Borg, A., Abrahamsson H. Endwall convective heat transfer for bluff bodies, *International Communications in Heat and Mass Transfer*, 2012, **39**(2), pp. 167-173.

[27] Duchaine, F., Boileau, M., Sommerer, Y., Poinsot, T., Large eddy simulation of flow and heat transfer around two square cylinders in a tandem arrangement, *Journal of Heat Transfer*, 2014, **136**(10), p. 101702.
[28] Jacobi, A.M., Shah, R.K., Heat transfer surface enhancement through the use of longitudinal vortices: a review of recent progress, *Experimental Thermal and Fluid Science*, 1995, **11**(3), pp. 295-309.
[29] Tiggelbeck, S., Mitra, N.K., Fiebig M. Comparison of wing-type vortex generators for heat transfer enhancement in channel flows, *ASME Journal of Heat Transfer*, 1994, **116**(4), pp. 880-885.
[30] Fiebig, M., Vortices, generators and heat transfer, *Chemical Engineering Research and Design*, 1998, **76**(2), pp. 108-123.
[31] Velte, C.M., Hansen, M.O., Okulov, V.L., Helical structure of longitudinal vortices embedded in turbulent wall-bounded flow, *Journal of Fluid Mechanics*, 2009, **619**, pp. 167-177.
[32] You, D., Wang, M., Mittal, R., Moin, P., Large-eddy simulations of longitudinal vortices embedded in a turbulent boundary layer, *AIAA Journal*, 2006, **44**(12), p. 3032.
[33] Lu, F.K., Pierce, A.J., Shih, Y., Liu, C., Li, Q., Experimental and numerical study of flow topology past micro vortex generators, *AIAA paper*, 2010, Paper No. 2010-4463.
[34] Wroblewski, D.E., Eibeck, P.A., Measurements of turbulent heat transport in a boundary layer with an embedded streamwise vortex, *International Journal of Heat and Mass Transfer*, 1991, **34**(7), pp. 1617-1631.
[35] Biswas, G., Chattopadhyay, H., Heat transfer in a channel with built-in wing-type vortex generators, *International Journal of Heat and Mass Transfer*, 1992, **35**(4), pp. 803-814.
[36] Gentry, M., Jacobi, A., Heat transfer enhancement by delta-wing-generated tip vortices in flat-plate and developing channel flows, *ASME Journal of Heat Transfer*, 2002, **124**, pp. 1158-1168.
[37] Wang, C., Luo, L., Wang, L., Sundén, B., Effects of vortex generators on the jet impingement heat transfer at different cross-flow Reynolds numbers, *International Journal of Heat and Mass Transfer*, 2016, **96**, pp. 278-286.
[38] Wang, C., Wang, L., Sundén, B., A novel control of jet impingement heat transfer in cross-flow by a vortex generator pair, *International Journal of Heat and Mass Transfer*, 2015, **88**, pp. 82-90.
[39] Oneissi, M., Habchi, C., Russeil, S., Bougeard, D., Lemenand, T., Novel design of delta winglet pair vortex generator for heat transfer enhancement, *International Journal of Thermal Sciences*, 2016, **109**, pp. 1-9.
[40] Ghorbani-Tari, Z., Wang, L., Sunden, B., Experimental study of heat transfer characteristics of a bluff body interacting with a rib by using liquid crystal thermography, *ASME International Mechanical Engineering Congress and Exposition*, 2013, Paper No. IMECE2013-64328.
[41] Ghorbani-Tari Z, Wang, L., Sunden, B., Heat transfer characteristics around an obstacle controlled by the presence of ribs, *Department of Energy Sciences, Lund University, Sweden,*2014, Internal Report No. HT1403.
[42] Sunden, B., Ghorbani-Tari, Z., Wang, L., Heat Transfer Characteristics around an Obstacle Controlled by the Presence of Ribs, *Heat Transfer Research*, 2016, **47**(10), pp. 893-906.

[43] Ghorbani-Tari, Z., Sunden, B., Experimental study of heat transfer control around an obstacle by using a rib, *Heat Transfer Research*, 2016, **47**(8), pp. 781-795.
[44] Allison, C., Dally, B., Effect of a delta-winglet vortex pair on the performance of a tube–fin heat exchanger, *International Journal of Heat and Mass Transfer*, 2007, **50**(25), pp. 5065-5072.
[45] Du, X., Feng, L., Yang, Y., Yang, L., Experimental study on heat transfer enhancement of wavy finned flat tube with longitudinal vortex generators, *Applied Thermal Engineering*, 2013, **50**(1), pp. 55-62.
[46] Fiebig, M., Kallweit, P., Mitra, N., Tiggelbeck, S., Heat transfer enhancement and drag by longitudinal vortex generators in channel flow, *Experimental Thermal and Fluid Science*, 1991, **4**(1), pp. 103-114.
[47] Joardar, A., Jacobi, A., Heat transfer enhancement by winglet-type vortex generator arrays in compact plain-fin-and-tube heat exchangers, *International Journal of Refrigeration*, 2008, **31**(1), pp. 87-97.
[48] Biswas, G., Mitra, N., Fiebig, M., Heat transfer enhancement in fin-tube heat exchangers by winglet type vortex generators, *International Journal of Heat and Mass Transfer*, 1994, **37**(2), pp. 283-291.
[49] Fiebig, M., Valencia, A., Mitra, N., Wing-type vortex generators for fin-and-tube heat exchangers, *Experimental Thermal and Fluid Science*, 1993, **7**(4), pp. 287-295.
[50] Sinha, A., Chattopadhyay, H., Iyengar, A.K., Biswas, G., Enhancement of heat transfer in a fin-tube heat exchanger using rectangular winglet type vortex generators, *International Journal of Heat and Mass Transfer*, 2016, **101**, pp. 667-681.
[51] He, J., Liu, L., Jacobi, A., Air-side heat-transfer enhancement by a new winglet-type vortex generator array in a plain-fin round-tube heat exchanger, *Journal of Heat Transfer*, 2010, **132**(7), p. 071801.
[52] Tang, L., Chu, W., Ahmed, N., Zeng, M., A new configuration of winglet longitudinal vortex generator to enhance heat transfer in a rectangular channel, *Applied Thermal Engineering*, 2016, **104**, pp. 74-84.
[53] Lemouedda, A., Breuer, M., Franz, E., Botsch, T., Delgado, A., Optimization of the angle of attack of delta-winglet vortex generators in a plate-fin-and-tube heat exchanger, *International Journal of Heat and Mass Transfer*, 2010, **53**(23), pp. 5386-5399.
[54] Jang, J.Y., Hsu, L.F., Leu, J.S., Optimization of the span angle and location of vortex generators in a plate-fin and tube heat exchanger, *International Journal of Heat and Mass Transfer*, 2013, **67**, pp. 432-444.
[55] Gokce, Z.O., Endwall shape modification using vortex generators and fences to improve gas turbine cooling and effectiveness, *PhD Thesis*, 2012, The Pennsylvania State University, USA.
[56] Hwang, J.J., Lia, D.Y., Tsia, Y.P., Heat transfer and pressure drop in pin-fin trapezoidal ducts, *ASME Journal of Turbomachinery*, 1998, **121**, pp. 264-271.
[57] Lau, S.C., Kim, Y.S., Han, J.C., Local endwall heat/mass-transfer distributions in pin fin channels, *Journal of Thermophysics and Heat Transfer*, 1987, **1**(4), pp. 365-372.
[58] Bianchini, C., Facchini, B., Simonetti, F., Tarchi, L., Zecchi, S., Numerical and experimental investigation of turning flow effects on innovative pin fin arrangements for trailing edge cooling configurations, *ASME Journal of Turbomachinery*, 2012, **134**(2), p. 021005.

[59] Lawson, S.A., Thrift, A.A., Thole, K.A., Kohli, A., Heat transfer from multiple row arrays of low aspect ratio pin fins, *International Journal of Heat and Mass Transfer*, 2011, **54**(17-18), pp. 4099-4109.
[60] Dabagh, A.M.A., Andrews. G., Pin-fin heat transfer: contribution of the wall and the pin to the overall heat transfer, *Proc. ASME International Gas Turbine and Aeroengine Congress and Exposition*, 1992. Paper No. 92-GT-242.
[61] Luo, L., Du, W., Wang, S., Sunden, B., Zhang, X., Flow structure and heat transfer characteristics of a 90°-turned pin-finned wedge duct with dimples at different locations, *Numerical Heat Transfer, Part A: Applications*, 2018, **73**(3), pp. 143-162.
[62] Luo, L., Wen, F., Wang, L., Sundén, B., Wang, S., On the solar receiver thermal enhancement by using the dimple combined with delta winglet vortex generator, *Applied Thermal Engineering*, 2017, **111**, pp. 586-598.
[63] York, R.E., Hylton, L.D., Mihelc, M.S., An experimental investigation of endwall heat transfer and aerodynamics in a linear vane cascade, *Journal of Engineering for Gas Turbines and Power*, 1984, **106**(1), pp. 159-167.
[64] Luo, L., Wang, C., Wang, L., Sundén, B., Wang, S., Endwall heat transfer and aerodynamic performance of bowed outlet guide vanes (OGVs) with on-and off-design conditions, *Numerical Heat Transfer, Part A: Applications*, 2016, **69**(4), pp. 352-368.
[65] Sieverding, C.H., Wilputte, P., Influence of mach number and end wall cooling on secondary flows in a straight nozzle cascade, *ASME Journal of Engineering for Power*, 1981, **103**(2), pp. 257-263.
[66] Jabbari, M.Y., Marston, K.C., Eckert, E.R.G., Goldstein, R.J., Film cooling of the gas turbine endwall by discrete-hole injection, *Journal of Turbomachinery*, 1996, **118**(2), pp. 278-284.
[67] Bogard, D.G., Thole, K.A., Gas turbine film cooling, *Journal of Propulsion and Power*, 2006, **22**(2), pp. 249-270.
[68] Wang, J., Wang, X., Zhao, L., He, F., Ma, S., Hao, C., An experimental and numerical investigation on endwall film cooling, *ASME Turbo Expo Turbine Technical Conference and Exposition*, June 3-7, 2013, San Antonio, Texas, USA, Paper No. GT2013-94267.
[69] Langston, L.S., Crossflows in a turbine cascade passage, *ASME Journal of engineering for power*, 1980, **102**(4), pp. 866-874.
[70] Sieverding, C.H., Van den Bosche, P., The use of coloured smoke to visulize secondary flows in a turbine-blade cascade, *Journal of Fluid Mechanics*, 1983, **134**, pp. 85-89.
[71] Wang, H.P., Olson, S.J., Goldstein, R.J., Eckert, E.R.G., Flow visualization in a linear turbine cascade of high performance turbine blades, *Journal of Turbomachinery*, 1997, **119**(1), pp. 1-8.
[72] Zess, G.A., Thole, K.A., Computational design and experimental evaluation of using a leading edge fillet on a gas turbine vane, *ASME Journal of Turbomachinery*, 2001, **124**, pp. 167-175.
[73] Shih, T.I.P., Lin, Y.L., Controlling secondary-flow structure by leading-edge airfoil fillet and inlet swirl to reduce aerodynamic loss and surface heat transfer, *ASME Journal of Turbomachinery*, 2003, **125**, pp. 48-56.
[74] Mahmood, G.I., Acharya, S., Experimental investigation of secondary flow structure in a blade passage with and without leading edge fillets, *Journal of Fluids Engineering*, 2007, **129**(3), pp. 253-262.

[75] Saha, R., Fridh, J., Fransson, T., Mamaev, B.I., Annerfeldt, M., Experimental studies of leading edge contouring influence on secondary losses in transonic turbines, *Proc. ASME Turbo Expo,* June 11-15, 2012, Copenhagen, Denmark, Paper No. GT2012-68497.

[76] Dossena, V., Perdichizzi, A., Savini, M., The influence of endwall contouring on the performance of a turbine nozzle guide vane, *ASME Journal of Turbomachinery*, 1999, **121**, pp. 201-208.

[77] Yan, J., Gregory-Smith, D.G., Walker, P.J., Secondary flow reduction in a nozzle guide vane cascade by non-axisymmetric end-wall profiling, *ASME International Gas Turbine and Aeroengine Congress and Exhibition*, 1999, p. V001T003A051-V001T003A051.

[78] Shih, T.I-P., Lin, Y.L., Simon, T.W., Control of Secondary Flows in a Turbine Nozzle Guide Vane by Endwall Contouring, *ASME Turbo Expo: Power for Land, Sea, and Air: American Society of Mechanical Engineers*; 2000, Paper No. 2000-GT-0556.

[79] Taremi, F., Sjolander, S.A., Praisner, T.J., Application of endwall contouring to transonic turbine cascades: Experimental Measurements at design conditions, *Journal of Turbomachinery*, 2013, **135**(1), p. 011031.

[80] Saha, A.K., Acharya, S., Computations of turbulent flow and heat transfer through a three-dimensional nonaxisymmetric blade passage, *Journal of Turbomachinery*, 2008, **130**(3), p. 031008.

[81] Milidonis, K.F., Georgiou, D.P., Film cooling effectiveness in the region of the blade-endwall corner junction with the injection assisted by the recirculating vortex flow, *International Journal of Heat and Mass Transfer*, 2015, **83**, pp. 294-306.

[82] Doerffer, P., Flaszynski, P., Magagnato, F., Streamwise vortex interaction with a horseshoe vortex, *Journal of Thermal Science*, 2003, **12**(4), pp. 304-309.

[83] Mirmanto, H., Sasongko, H., Noor, D.Z., Reduction of energy losses in the end wall junction area through the addition of forward facing step turbulent generator, *Applied Mechanics and Materials: Trans. Tech. Pub*., 2014. pp. 256-261.

[84] Thrift, A.A., Thole, K.A., Influence of flow injection angle on a leading-edge horseshoe vortex, *International Journal of Heat and Mass Transfer*, 2012, **55**(17-18), pp. 4651-4664.

[85] Takeishi, K., Oda, Y., Seguchi, J., Kozono, S., Effect of endwall film cooling upstream of an airfoil/endwall junction to suppress the formation of horseshoe vortex in a symmetric airfoil. A*SME Turbo Expo: Turbine Technical Conference and Exposition*, 2013. Paper No. GT2013-95385.

[86] Wang, C., Luo, L., Wang, L., Sundén, B., Chernoray, V., Arroyo, C., Abrahamsson, H., Experimental and numerical investigation of outlet guide vane and endwall heat transfer with various inlet flow angles, *International Journal of Heat and Mass Transfer*, 2016, **95**, pp. 355-367.

[87] Wang, C., Wang, L., Sundén, B., Chernoray, V., Abrahamsson, H., An experimental study of heat transfer on an outlet guide vane, *Proc. ASME Turbo Expo*: *Turbine Technical Conference and Exposition,* June 16-20, 2014, Germany, Paper No. GT2014-25100.

[88] Barigozzi, G., Franchini, G., Perdichizzi, A., Quattrore, M., Endwall film cooling effects on secondary flows in a contoured endwall nozzle vane, *ASME Journal of Turbomachinery*, 2010, **132**(4), p. 041005.

[89] Lynch, S.P., Sundaram, N., Thole, K.A., Kohli, A., Lehane, C., Heat transfer for a turbine blade with nonaxisymmetric endwall contouring, *ASME Journal of Turbomachinery*, 2011, **133**(1), p. 011019.
[90] Barigozzi, G., Franchini, G., Perdichizzi, A., Ravelli, S., Film cooling of a contoured endwall nozzle vane through fan-shaped holes, *International Journal of Heat and Fluid Flow*, 2010, **31**(4), pp. 576-585.
[91] Lynch, S.P., Thole, K.A. ,The effect of combustor-turbine interface gap leakage on the endwall heat transfer for a nozzle guide vane, *ASME Journal of Turbomachinery*, 2008, **130**(4), p. 041019.
[92] Thrift, A.A., Thole, K.A., Hada, S., Effects of orientation and position of the combustor-turbine interface on the cooling of a vane endwall, *ASME Journal of Turbomachinery*, 2012, **134**(6), p. 061019.
[93] Du, K., Li, Z., Li, J., Effects of the leading edge injection slot on the film cooling and heat transfer performance of the vane endwall, *International Journal of Heat and Mass Transfer*, 2016, **102**, pp. 1308-1320.
[94] Du, K., Li, Z., Li, J., Sunden, B., Influence of the upstream slot geometry on the endwall cooling and phantom cooling of vane suction side surface, *Applied Thermal Engineering*, 2017, **121**, pp. 688-700.
[95] Wang, C., Experimental study of outlet guide vane heat transfer and gas turbine internal cooling, 2016, *PhD Thesis,* Lund University, Sweden.
[96] Schlichting, H., Boundary-Layer Theory, 7th ed., 1979, McGraw-Hill, New York.
[97] Winterton R.H.S., Where did the Dittus and Boelter equation come from?, *International journal of heat and mass transfer*, 1998, **41**(4-5), pp. 809-810.
[98] Hwang, J.J., Lui, C.C., Measurement of endwall heat transfer and pressure drop in a pin-fin wedge duct, *International Journal of Heat and Mass Transfer*, 2002, **45**(4), pp. 877-889.
[99] Menter, F.R., Review of the shear-stress transport turbulence model experience from an industrial perspective, *International journal of computational fluid dynamics*, 2009, **23**(4), pp. 305-316.
[100] Du, W., Luo, L., Wang, S., Zhang, X., Flow structure and heat transfer characteristics in a 90-deg turned pin fined duct with different dimple/protrusion depths, *Applied Thermal Engineering*, 2019, **146**, pp. 826-842.
[101] Liao, G., Wang, X., Li, J., Zhang, F., A numerical comparison of thermal performance of in-line pin–fins in a wedge duct with three kinds of coolant, *International Journal of Heat and Mass Transfer*, 2014, **77**, pp. 1033-1042.
[102] Sundaram, N., Thole, K.A., Bump and trench modifications to film-cooling holes at the vane-endwall junction, *ASME Journal of Turbomachinery*, 2008, **130**(4), p. 041013.
[103] Hada, S., Thole, K.A., Computational study of a midpassage gap and upstream slot on vane endwall film-cooling, *ASME Journal of Turbomachinery*. 2011, **133**(1), p. 011024.
[104] Moffat, R.J. ,Describing the uncertainties in experimental results, *Experimental Thermal and Fluid Science*. 1988, **1**(1), pp. 3-17.
[105] Devenport, W.J., Simpson, R.L. Time-dependent and time-averaged turbulence structure near the nose of a wing-body junction, *Journal of Fluid Mechanics*, 1990, **210**, pp. 23-55.

[106] Metzger, D.E,, Haley, S.W., Heat transfer experiments and flow visualization for arrays of short pin fins, *Proc. ASME International Gas Turbine Conference and Exhibition*, 1982, New YorK, USA, Paper No. 82-GT-138.
[107] Chyu, M.K., Hsing, Y.C., Shih, T.I.P., Natarajan, V., Heat transfer contributions of pins and endwall in pin-fin arrays: effects of thermal boundary condition modeling, *ASME Journal of Turbomachinary*, 1999, **121**, pp. 257-263.

Printed by Media-Tryck, Lund 2019 NORDIC SWAN ECOLABEL 3041 0903

Faculty of Engineering
Lund University
ISBN 978-91-7895-048-5
ISSN 0282-1990
ISRN LUTMDN/TMHP-19/1145-SE